DESIGN AND OPTIMIZATION OF A SHAPE MEMORY ALLOY ACTUATED PUMP WITH THERMOFLUIDIC FEEDBACK

by

Matthew D. Pierce

A thesis submitted to the faculty of
The University of Utah
in partial fulfillment of the requirements for the degree of

Master of Science

Department of Mechanical Engineering

The University of Utah

May 2011

The University of Utah Graduate School

STATEMENT OF THESIS APPROVAL

The thesis of **Matthew D. Pierce**

has been approved by the following supervisory committee members:

Stephen A. Mascaro	, Chair	**3/15/2011** Date Approved
Mark A. Minor	, Member	**3/17/2011** Date Approved
William R. Provancher	, Member	**3/28/2011** Date Approved

and by **Timothy Ameel** , Chair of the Department of **Mechanical Engineering**

and by Charles A. Wight, Dean of The Graduate School.

ABSTRACT

This thesis presents the design and optimization of a biologically inspired wet shape memory alloy (SMA) actuated pump that can provide thermal energy via fluidic convection to actuate external wet SMA subsystems. Furthermore, the pump draws from its own fluidic output to assist in the actuation of its own internal SMA actuators. A thorough analysis of the previous wet SMA robotic heart is conducted by searching for opportunities for improvement. Methods of improving the pump's output-to-input ratio included modifying the pumping chambers, actuation cycle timing, implementing electrical actuation, and continuously adding heat to the system.

Dynamic modeling was performed to provide a baseline indicator of what was to be expected during actual implementation and testing. The effects of changing various parameters were explored to determine optimal configurations. Key parameters affecting performance include mechanical advantage, actuator length, flow durations, and water temperature.

Implemented design changes and testing confirmed the modeling results. Continuous heating of the hot water within the pressurized accumulator greatly enhanced the pump's performance. Using only fluidic induced actuation, the output-to-input ratio peaked at 1.4. The pump reached an output-to-input ratio of 2.1 with the aid of electrical actuation. This is the first successful implementation of a self-sustaining thermofluidically powered SMA pump. Furthermore, unlike other SMA micropumps that typically output 1 mL/min

or less, this pump is capable of a macroscale net output of 66 mL/min.

While the pump's output exceeds the required input, the power efficiency and power density of the pump do not compare to that of the human heart due to the amount of power required to keep the hot water continuously heated. Viable options for improving efficiency and power density include minimizing pump mass, optimizing pumping chamber design, and reducing the amount of heat necessary to keep the hot water at an elevated temperature.

TABLE OF CONTENTS

LIST OF TABLES

LIST OF FIGURES

ACKNOWLEDGEMENTS

While I have spent many months working on the research presented in this thesis, I could not have done it without the help and support of family, friends, and colleagues. I would like to thank my advisor, Dr. Stephen Mascaro, for meeting often with me and providing the advice necessary to develop the research in a positive and constructive way. I would also like to thank Les Flemming and Ronnie Boutte for all the help they have provided over the years when I was stuck and couldn't figure out the next step to take in the research.

I would like to express my appreciation to all of the members of the BioRobotics lab who spent countless hours helping out, keeping me company, and simply providing great conversation. It made the time spent seem so much quicker. Without their help, I would still be sitting at my desk working on the research.

I give thanks to Kelly Perkins for working with me over the years and being flexible in allowing me to complete my research in a timely manner. He has always supported me in my academic endeavors.

Finally, I would like to express love and special thanks to my dear wife, Michelle, who has put up with me over the years and supported me in my efforts to become a better person in every way. Without her consistent support and sincere interest in my success, I wouldn't accomplish anything.

CHAPTER 1

INTRODUCTON

1.1 Motivation

As the field of robotics evolves, it is imperative to develop new technology for better ways to actuate and control the robots to perform more complicated tasks. These robots are controlled in a variety of ways. Common methods of actuation include the use of electrical motors, pneumatics and hydraulics. Smart materials such as electroactive polymers (EAPs) and shape memory alloys (SMAs) are becoming increasingly popular in robotics due to their similarity to muscle [1] and their high biocompatibility [2]. This makes them good candidates for hand and facial prosthetics research [3, 4]. In addition to their biocompatibility, there are also many other advantages to using SMA actuators for nonbiological mechanisms including thermostats [5], adaptive wings [6], and even humanoid robots [7, 8].

Shape memory alloys function based on the heating and cooling of smart materials that behave differently based on temperature. As heat is applied, typically by Joule heating, a nonlinear phase transformation occurs and begins to exhibit a shape-memory effect where the material transforms to a previous geometry. The most common type of SMA is nitinol, a nickel-titanium based alloy. At room temperature, nitinol is in a martensitic phase and as heat is applied, it transforms to an austenitic phase. This phase

transformation between martensite and austenite generally exhibits a contracting strain similar to muscle. It is this muscle-like actuation that makes SMAs desirable for the development of biologically inspired robots.

Shape memory alloys are commonly used for applications that do not require high reciprocation rates due to their limited bandwidth. This is due to the difficulty of heating and cooling the SMA quickly and efficiently. For this reason, the wet SMA actuator was developed to allow for more efficient actuation and increased rates using forced convection [9]. Using forced convection, SMA actuators have been developed that can achieve efficiency of up to 3% [10]. Other estimates suggest efficiencies of 0.2% when considering heat loss to the surroundings [11].

Figure 1.1 is a diagram of the wet SMA actuator concept. A wet SMA actuator consists of SMA wire enveloped in fluid that is contained within a compliant tube. This compliance allows for the actuator to expand and contract with minimal spring resistance. The fluid inlet of the actuator is connected to a terminal that is supplied with hot or cold fluids and the outlet is connected to a terminal that dumps the used fluid into a lower

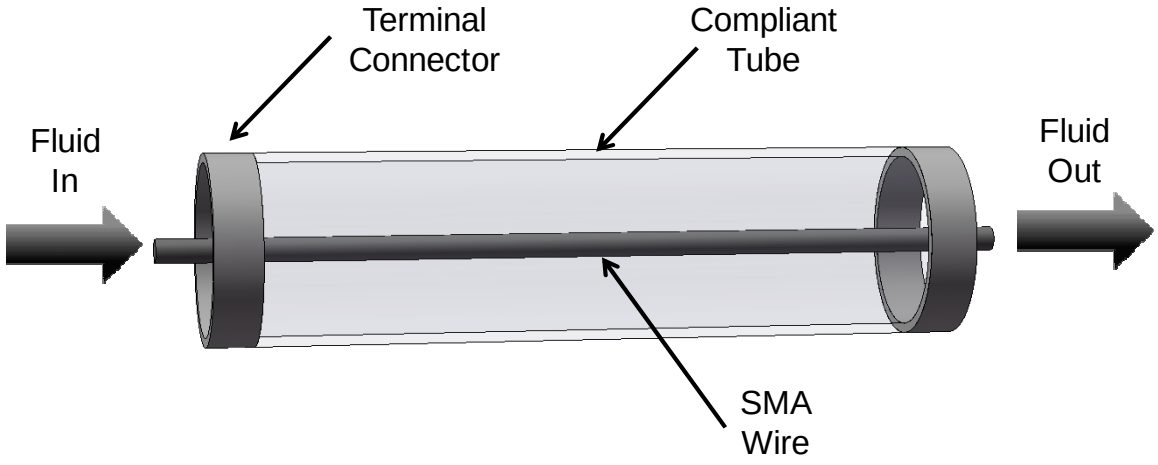

Figure 1.1 Wet SMA actuator design concept.

pressure reservoir. Entire wet SMA actuator arrays have been used to control hand and finger movement [12] and could be used to control other high degree-of-freedom mechanisms as well.

As more biologically inspired mechanisms are being developed using wet SMA, it is necessary to develop methods of making these robots more mobile and self-sustaining. One step towards enabling these wet SMA robots is the development of an onboard pump that can provide heating and cooling to sustain the actuation of external subsystems using wet SMA technology. Just as the wet SMA actuators behave like muscles with a cardiovascular system, a wet SMA pump would be analogous to a heart. One unique attribute of the heart is that it is able to pump blood and provide energy to the muscles of the heart itself, forming a self-sustaining pumping system. In the same way, the SMA pump would need to be able to provide energy to sustain self-actuation in addition to that of external wet SMA systems as shown in Figure 1.2. One such device has previously been designed and implemented by Joel Ertel [13, 14], but the output performance was not sufficient to even sustain self-actuation of its own wet SMA actuators. In order for

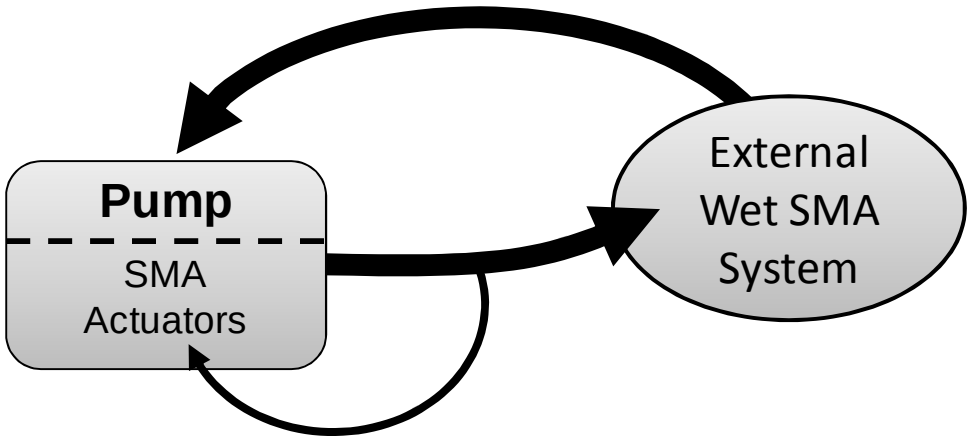

Figure 1.2 Diagram demonstrating a pump that provides energy to external systems and itself, forming a self-sustaining pump analogous to a heart.

such a device to be viable for external subsystems, the amount of fluid output of the pump must be greater than the amount of fluid input required to cause actuation for the pumping action.

The objective of this thesis is to create a biologically inspired wet shape memory alloy actuated pump, or heart, that can provide thermal energy via fluid convection to external wet SMA subsystems. Furthermore, the pump should draw from its own thermofluidic output to assist in actuating its own internal SMA actuators. By conducting a thorough analysis of the previous wet SMA robotic heart, opportunities for improvement arise to design a pump with a higher output-to-input performance. This can be accomplished by redesigning the pumping chamber diaphragm, developing more efficient ways to actuate the SMA with fluid timing, implementing electrical actuation in combination with the fluidic actuation, and continuous heat addition. Careful modeling, implementation, and testing are necessary in order to verify the increased performance of the pump over that of the previous design. Through characterization of this SMA pump's performance, a comparison can be drawn between other types of pumps including the human heart to gain insight as to how the SMA pump actually performs.

1.2 Review of Existing Pump Technology

Pumps have been used for centuries to transport fluids from one location or state to another. Most types of pumps fall under two main categories: dynamic pumps and positive displacement pumps. Dynamic pumps are called dynamic pumps because the volume output of the pump may vary depending on the speed of operation. Generally, as the speed increases, the output efficiency of the pump decreases. The attractive features of dynamic pumps are high flow rates and high power densities. Centrifugal and axial

pumps are common classes of dynamic pumps [15].

Positive displacement pumps, on the other hand, function by displacing a fixed volume of fluid independent of the operating speed. They work by trapping fluid and moving it from the inlet of the pump to the outlet. This can be done continuously or intermittently, depending on the type of pump. Generally, these types of pumps operate at low speeds and have high outputs and efficiencies, but have low power densities due to their larger sizes. Reciprocating, rotary, and metering pumps are typical types of positive displacement pumps.

As there are many different types of pumps available, each has a unique set of characteristics that make them the best for a certain type of job. Piston and diaphragm pumps are well-suited for pumping gases or light liquids, while heavy duty pumps such as screw pumps are designed for pumping heavy viscous fluids or soft materials. Some require daily maintenance or high amounts of energy to operate properly while others are guaranteed to function without problem for multiple years before needing replacement such as a refrigerator compressor. Some pumps are required to pump thousands of gallons of waste or fluid per day [16], whereas others are needed to deliver small doses of insulin to patients with diabetes [17].

When it comes to determining which type of pump the wet SMA pump should be, many factors should be considered. The primary requirement is that the pump should be able to operate using wet SMA actuators as the principle driving mechanism. This places difficulty on using dynamic and rotary pumps since high speeds will be unattainable. Conversely, positive displacement pumps typically operate at slow speeds and can operate by a change in geometry. Reciprocating, progressive cavity, and peristaltic pumps

all seem to be viable options at this point.

The second main requirement of the wet SMA pump is that it must be able to operate using fluid that it pumps itself. As mentioned in section 1.1, the goal of this research is to be able to pump more fluid than is required to cause actuation. In order to achieve this performance, different types of pumps must be analyzed discriminating by the volume output per unit strain of the wet SMA actuator. This will be discussed in more detail in section 3.1 where a diaphragm pump, peristaltic pump, and dual-bellows pump will all be analyzed for output performance.

Output performance is the primary goal of the thesis, but power efficiency and power density of the wet SMA pump are also of interest, especially with respect to the human heart. Figure 1.3 compares different types of pumps with respect to their efficiencies and power densities including the human heart. Due to the widespread application of each type of pump, it is difficult to highlight the exact regions where each type of pump

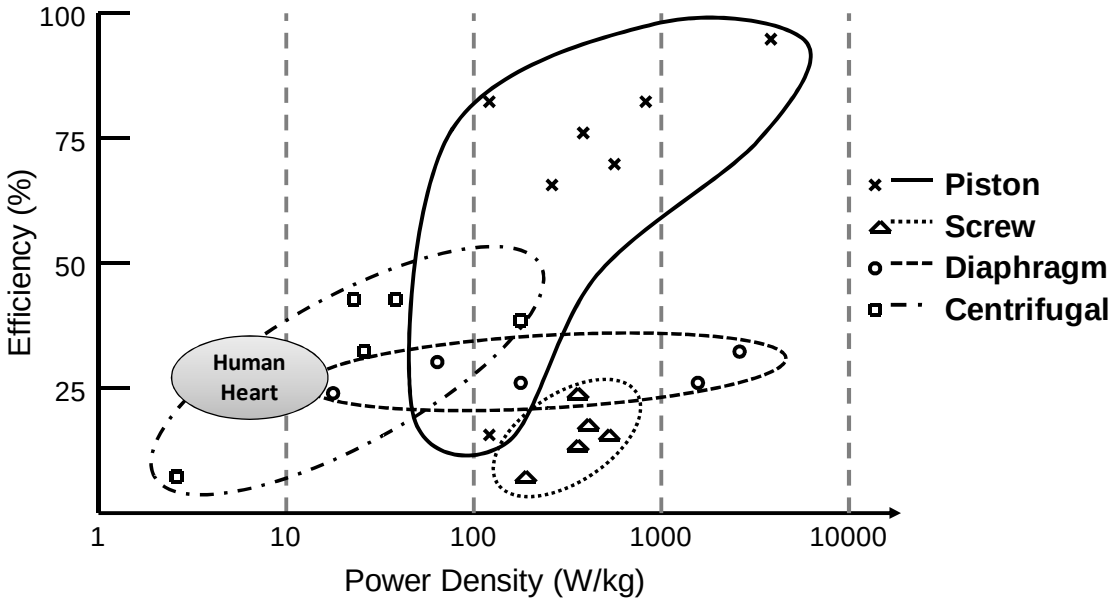

Figure 1.3 Efficiency and power density regions of common types of pumps with respect to the human heart. See Appendix A for more details.

operates, but this figure provides a general idea of what common pumps are currently available to the public. Appendix A provides detailed information on each data point represented in the figure.

With respect to the wet SMA pump, it is desirable to reach a performance level similar to that of the human heart. The human heart is capable of pumping with an efficiency between 18% - 35%, depending on age, weight, and other physical conditions [18]. The heart is generally considered to be a positive displacement reciprocating diaphragm pump, the same type of pump as the current wet SMA pump. By engineering the wet SMA pump to reach a similar level of efficiency, the end goal of creating a biologically inspired pump becomes more of a reality.

1.2.1 SMA Pumps

Although the wet SMA pump presented in this thesis is the first of its kind to be able to successfully utilize its own pumping output to sustain continued pumping, many other SMA pumps have been created on a micro scale. In general, these micropumps are used for delivering microliters of medicine on demand. Thin-film SMA micropumps have been developed that are capable of high reciprocation rates [19, 20]. One thin-film SMA diaphragm pump is capable of pumping up to 50 μL/min of water [21, 22]. A novel reciprocating peristaltic pump prototype is capable of outputs up to 1000 μL/min of fluid using SMA springs [23-25]. Another application of SMA micropumps is for chemical delivery to biochemical integrated circuit chips [26, 27]. Since the robotic heart must be able to actuate external wet SMA systems on a macroscale, high net volume outputs on the order of mL/min are necessary. This would make the wet SMA pump the first pump to be able to provide thermal fluids to external wet SMA subsystems on a macroscale.

1.3 Thesis Overview

Although some research has been performed for large scale SMA pumps by Ertel, the results have been less than satisfactory for self-sustainment and actuation of other external wet SMA mechanisms. This thesis will discuss previous research performed, elucidate the drawbacks and opportunities for improvement on previous designs, and discuss the details and results of the improvements made.

Chapter 2 will explain the conceptual design of a SMA robotic pump, discuss the original implementation and results, and highlight the opportunities for improvement upon output performance. Some areas for improvement include the pumping chamber, actuation timing, heat loss minimization, and heat addition. Details of the improvements made to the preexisting design will be discussed in Chapter 3. Equations, models, and figures will be provided to support each improvement.

Chapter 4 will discuss the optimization of parameters by modeling and simulation. Improvements to the existing model will be discussed in conjunction with the addition of Joule heating. Simulation results will be used to provide the optimal sets of parameters necessary to exceed an output-to-input ratio greater than 1.0.

Chapter 5 will describe the proof-of-engineering prototype with all of the previously discussed improvements and provide the experimental results. A discussion of the comparison of the simulation and experimental results will be provided. Results will consist of fluid-only actuation and electrical actuation. Power requirements will also be discussed.

Chapter 6 will conclude this thesis with discussion of the results and recommendations for future research.

CHAPTER 2

REVIEW OF THE ORIGINAL SMA PUMP DESIGN

In order to improve the performance of the SMA robotic heart, it is imperative to review the previous pump design [13] and map out the strengths and weaknesses of its key concepts, components and features. Although the original design had undergone its own optimization process by varying actuator length, flow duration, and accumulator pressure, there are still several untried approaches that could improve the overall performance of the robotic pump. Varying mechanical advantage had not been explored nor had using actuator lengths longer than 30 cm. The only actuator lengths used were 20 cm and 30 cm. By using longer actuators, using longer flow duration would be necessary to find an optimal output for each actuator length. Electrical actuation was not explored.

The pump's performance is measured by the total volume output of pumping mechanism compared to the total required input for actuation to occur. This is referred to as the output-to-input ratio, or Q_{in}/Q_{out}. As mentioned in the previous chapter, it is desirable to obtain a higher output than input in order to sustain self-actuation and provide fluids to additional external subsystems. This chapter will discuss the key features of the previous design and will indicate areas for improvement that would result in overall increased output performance.

2.1 Design Concept

Many features comprise the entire robotic pump system. As with all pumps, there needs to be a mechanism that causes fluid volume displacement from one location to another. There are multiple variations of pumps that can perform this action. The type chosen for this application was a reciprocating positive displacement piston/diaphragm pump. A schematic of the entire system is shown in Figure 2.1. Since the pump has to be able to provide both hot and cold fluids to other subsystems, there are two separate pumping systems. Each pump system has an accumulator, a reservoir, a pumping chamber, and timed valves. The accumulators provide the pressure necessary to force the fluids through the tubing of separate subsystems and across the SMA actuators attached to the pumping chambers. The reservoirs hold the fluids after they have passed through any subsystem or pumping chamber actuator. The pumping chambers obtain the fluid

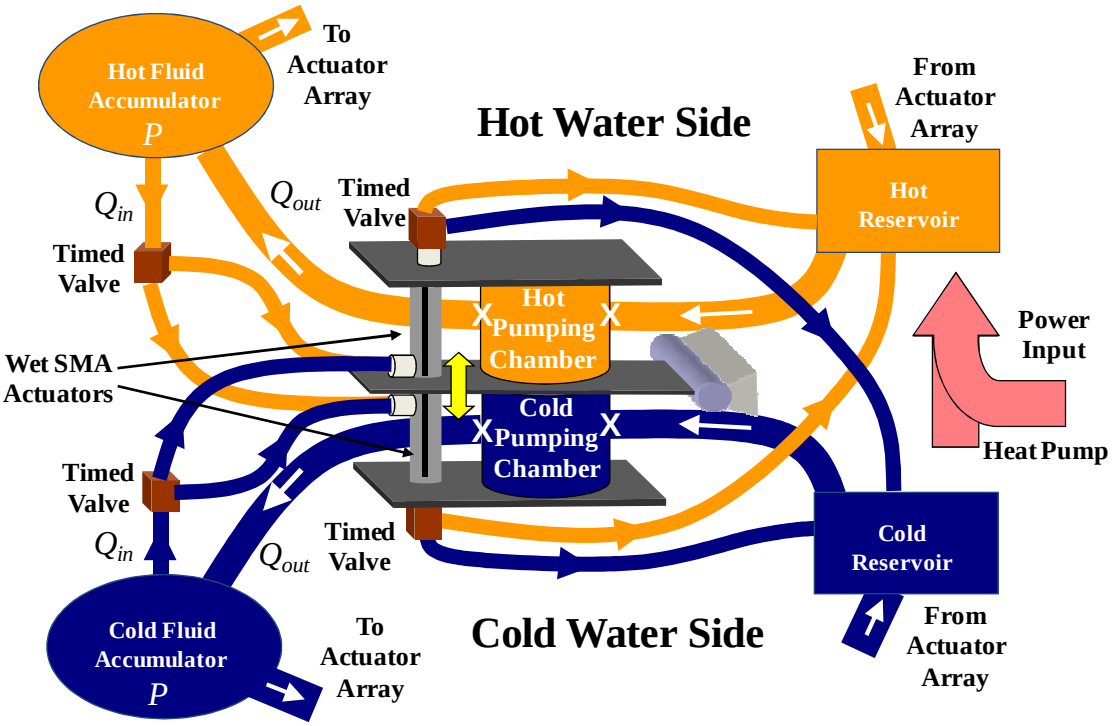

Figure 2.1 Modified conceptual design schematic of Ertel's robotic pump [13].

from the reservoirs and pump it back to the accumulators with the aid of check valves to ensure unidirectional flow. A set of timed valves control when hot and cold fluid are passed to the pumping chamber actuators while a different set of timed valves control the separation of hold and cold fluid into their respective reservoirs.

In this conceptual arrangement, the pumping chambers share a common lever that allows the SMA actuators to use mechanical advantage to increase displacement at the expense of force and vice versa. This allows for variation in accumulator pressure while still being able to cause some displacement in the pumping chambers. This arrangement also requires that the hot and cold chambers pump 180° out of phase to avoid any unwanted additional tension on the SMA actuators.

A primary requirement for this pump is that it must be able to pump fluids over an extended period of time without adding additional fluid. In order to accomplish this, heat must be added to the system, otherwise heat would eventually be lost and the pump would no longer perform at an optimal level. One way to maintain the heat necessary to cause SMA actuation is to continually add energy to the system. In this conceptual design, heat is being added to the hot reservoir by adding heat from an outside source and also taking heat from the cold reservoir.

2.2 Implementation and Results

Ertel's implementation prototype of the design concept discussed in section 2.1 is shown in Figure 2.2. The two pumping chambers are stacked vertically and share a common lever upon which the SMA actuators act. The accumulators and reservoirs rested at the foot of the pump and timing valves were placed near the entrance and exit points of the SMA actuators. The actuator inlets were located on the top and bottom of

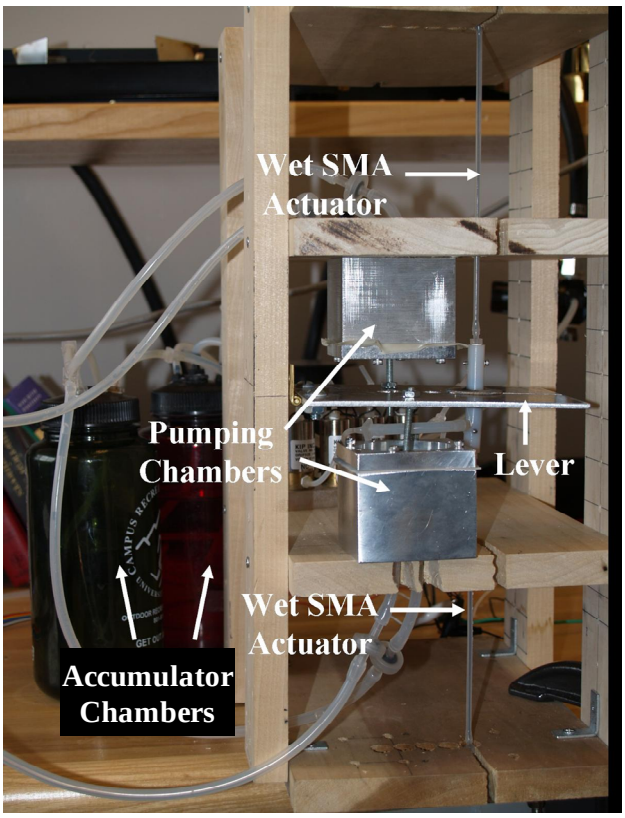

Figure 2.2 Previous implementation prototype of the SMA robotic pump mechanism.

the upper and lower SMA actuators, respectively. This arrangement required much tubing to stretch from the accumulators to the inlets and also from the reservoirs to the pumping chambers and back to the accumulators.

Prior to implementation, thermodynamic and kinematic modeling had been performed in an attempt to predict the output performance of the robotic pump. This was achieved using Matlab ODE solver software. The model allowed for design parameters such as accumulator pressure, pump reciprocation rate, mechanical advantage, SMA actuator length, and fluid properties to be varied in order to find a set of optimal parameters that would yield the highest output-to-input ratio. Figure 2.3 shows the output-to-input ratio comparison of the simulation model to actual experimental results for 30 cm actuators. In this figure, the output-to-input ratio was recorded for varying

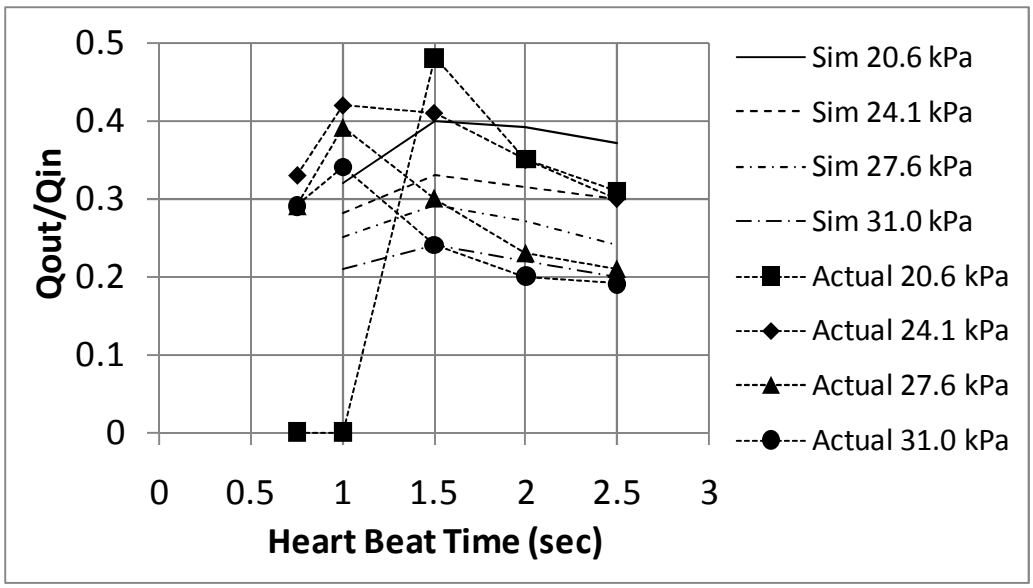

Figure 2.3 Previous simulation and experimental output-to-input ratio results comparison using 30 cm actuators using data from [13].

reciprocation rates and accumulator pressures. The simulation results do not agree exactly with the actual experimental results.

The simulation results suggest that lower accumulator pressures are desirable for increased performance, but the actual experimental results demonstrate that there is a midrange pressure that causes improved output performance. This model discrepancy could be attributed to factors unaccounted for such as varying fluidic properties over temperature as well as oversimplified assumptions made about the SMA actuators and its hysteresis. Other factors could include physical parameters of the pump such as fluidic capacitance in the tubes and chambers.

2.3 Limitations

The previous realization of the robotic heart had achieved a maximum output-to-input ratio of 0.47 at a single set of parameters, but this is not sufficient if the system is to

continuously supply fluids to itself and other subsystems without fluid addition. Fortunately, some opportunities in the previous design and implementation allow for improvement. Ertel has indicated some areas for improvement that may prove useful, but there are also some other ways of improving the performance that are not mentioned such as changing the pump chamber parameters, using other actuator lengths, altering the flow duration and timing, and minimizing heat loss. This section will describe the various limitations of the previous robotic pump design that suggest opportunities for improvement so as to increase the efficiency and performance of the system.

2.3.1 Pumping Chamber

An important area for improvement of the pump is the pumping chamber. Although the ideal piston-cylinder reciprocating pump can be efficient, its implementation can have a crippling affect on the performance of the pump. In the previous prototype, the piston was attached to the chamber with a 0.508 mm thick sheet, or diaphragm, of rubber. The sheet was slackened in order to decrease the resistance during the piston stroke. These factors caused significant bulging to occur on the order of milliliters during strokes. This bugling of the rubber diaphragm results in a considerable loss of output to the system, thus, reducing its output-to-input performance.

2.3.2 Actuation Timing

In the previous prototype, the working fluid was constantly flowing. Although hot water was passing through one actuator, cold water was passing through the other. There was no waiting period to allow the stagnant hot water to continue to induce actuation without being forced across the wire in the actuators. By implementing more complex

timing and control of the switch valves that allows for heat transfer during non-forced flow, there is an opportunity to decrease the input flow, thus increasing the output-to-input ratio.

2.3.3 Water as the Working Fluid

One of the most crucial limitations on the performance of the pump is the temperature of the working fluid relative to the transformation temperature of the SMA. The current pump design uses water, taking advantage of its low viscosity and large heat capacity. However, due to its relatively low boiling point – especially at higher elevations, the actuation does not reach its full stroke potential. The SMA actuators need to undergo a more complete phase transformation to austenite in order to capitalize on the strain capabilities of 4%. This poses need for alternate working fluids or electrical actuation. Alternate fluids would need to have high boiling points, low viscosities of the entire temperature range, high thermal conductivity coefficients, and be able to transport thermal energy to the actuators efficiently. With the help of electrical actuation, the total input required would decrease and yield a higher output-to-input performance.

2.3.4 Heat Loss

Due to the nature of the prototype, long tubing is required to transport the working fluid between the accumulators, SMA actuators, reservoirs, and pumping chambers. This results in significant heat surrendering to the environment. By the time the fluid reaches the actuators from the accumulators, the fluid will have lost a considerable amount of heat, thus reducing the actuation potential. By redesigning the implementation of the prototype, it is possible to decrease this heat loss and secure a higher temperature input to

the SMA actuators.

2.3.5 Heat Addition and Recycling

Continuously adding heat to the hot fluid in the system would ensure that the pump is able to continue to function properly over prolonged periods of time. Although Ertel did introduce the concept of being able to add heat and recycle the used fluids back into the system, it was never implemented in the physical prototype. This thesis includes the design and implementation of the concept of heat addition and recycling. Results will also be provided and discussed in Chapter 5.

2.4 Conclusions

By means of analyzing the previous pump design, many possible areas for improved performance have become evident. By careful examination and implementation of these modifications to the design, a higher performance is anticipated in both the modeling and experimental results. Detailed specifics about executing these changes are discussed in the following chapter.

CHAPTER 3

DESIGN IMPROVEMENTS

As limitations of the previous pump design have been identified, design and implementation of alternatives will now be discussed. In order to modify the SMA robotic pump and optimize the overall performance, a detailed analysis of each alternative proposal must be completed prior to selection. This chapter will focus on specific design modifications in each area of improvement mentioned in Chapter 2 that can be used to eliminate or reduce the affects of the limitations of the pump.

3.1 Pumping Chamber Designs

There are multiple approaches to redesigning the pumping chambers. These approaches include slightly modifying the current piston-cylinder or even completely changing the type of pump all together. While maximum output is preferred for design selection, all other considerations will be accounted for so as to craft the best overall performing pump in a reasonable manner.

3.1.1 Piston Diaphragm Pump

Perhaps the simplest way to modify the piston-cylinder design is to use a modified piston diaphragm. As mentioned in section 2.3.1, bulging in the diaphragm resulted in a

significant decrease in pumping output. One way to alleviate this bulging is to make the diaphragm much thicker. This alone would reduce bulging, but would also increase the stiffness that is imposed on the SMA actuators. In order lessen these stiffness effects, elastic groove hinges could be used around the perimeter of the chamber and the piston head. Figure 3.1 shows a cross section of how this works. Utilizing a finite-element analysis (FEA) approach, an optimal thickness could then be selected to reduce bulging while maintaining a relatively low stiffness along the actuation axis.

Using the material properties of Reoflex® 30 urethane rubber, finite element analysis provided in Figure 3.2 highlights that the displacement due to bulging yields a volume displacement less than 0.1 mL with a gage pressure of 15 kPa. The bulk of this bulging displacement occurs between the center of the diaphragm and the mating edge of the outer cylinder. By increasing the size of the center piston head, the bulging decreases significantly and the volume displacement per stroke also increases. The downfall to this is that the stiffness will also increase, causing unwanted strain on the SMA actuator. It

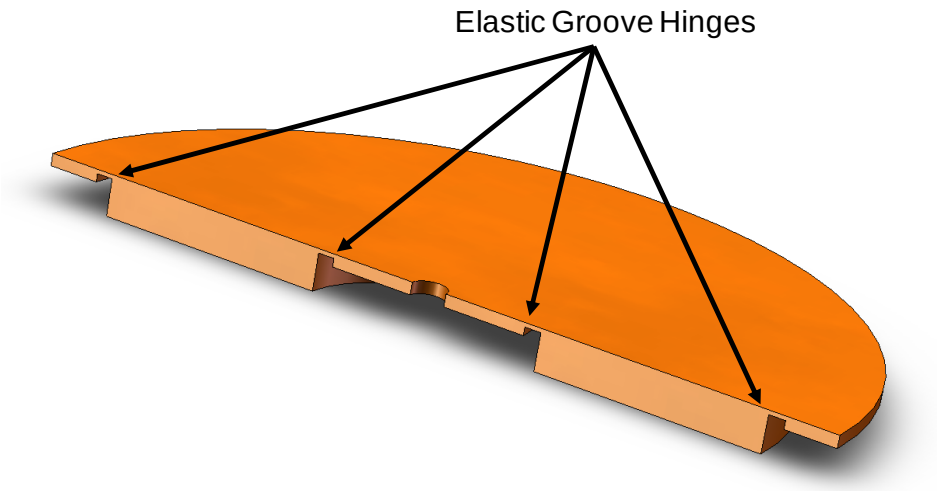

Figure 3.1 Cross section of the new diaphragm design indicating the elastic groove hinges.

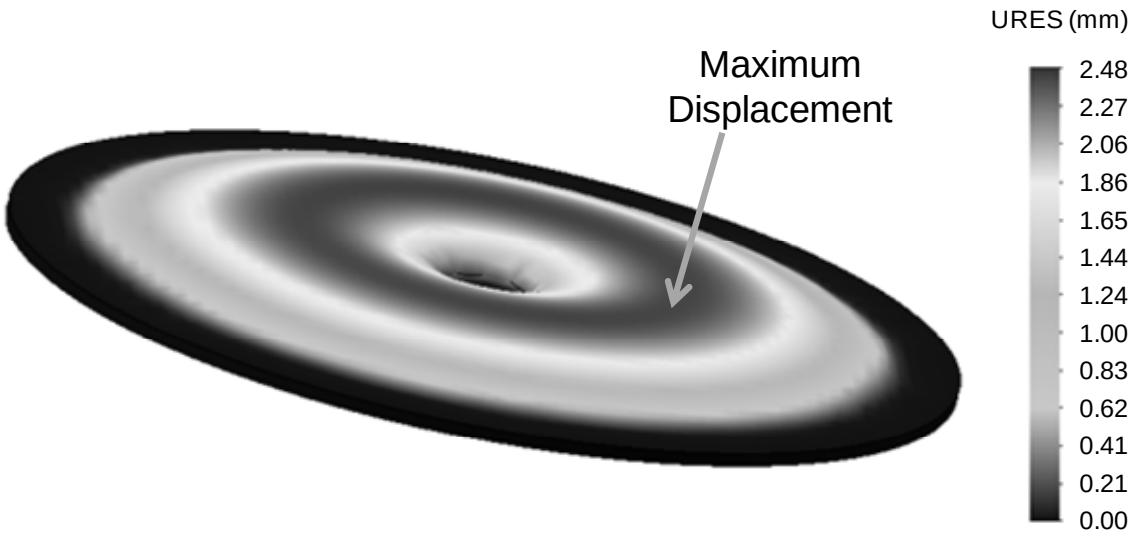

Figure 3.2 Finite element analysis of a diaphragm where the inner diameter restraint is $1/10^{th}$ of the outer diameter restraint. The volume displacement is less than 0.1 mL.

should be noted that the piston head diameter restraint used for the finite element analysis was $1/10^{th}$ the size of the outer piston chamber diameter restraint to obtain an acceptable estimate of the worst-case scenario of the bulging displacement.

It can be shown using a volumetric formula for a partial cone that the volume displacement per actuator strain is

$$\delta V = \frac{7\pi}{48} D^2 h \left(\frac{\delta l}{l}\right) \tag{3.1}$$

where δV is the volume displacement, D is the chamber diameter, h is the stroke, and $\delta l/l$ is the actuator strain which is 0.04, or 4%, at maximum. This equation evolves from a partial conical volume with an inner piston head diameter equal to ½ the pumping chamber diameter. As mentioned previously, increasing the piston diameter too much can cause an undesirable increase in diaphragm stiffness.

3.1.2 Peristaltic Pump

Using a peristaltic pump design is a completely different approach to increasing the pump output. This type of pump is more biologically inspired than the piston-cylinder. Similar to the heart, fluid is forced through tubes as the chamber contracts. In this case, fluid is forced along the direction of a cylindrical axis. Figure 3.3 is a conceptual diagram of how this functions with SMA actuators. A long compliant tube is wrapped with SMA wire and the working fluid enters the tube on one end through a check valve until the tube is full. When the wire contracts, the diameter of the tube decreases and forces the fluid through a check valve at the other end of the tube and into the accumulator.

The theoretical output of this design per strain can be approximated from the contraction of a diameter of a cylinder. The output is given by

$$\delta V = \frac{\pi}{2} D^2 h \left(\frac{\delta l}{l}\right) \tag{3.2}$$

where the parameters are the same as before with the conical piston diaphragm, except *h* is the compliant tube length. The leading fraction is almost 3.5 times larger than the

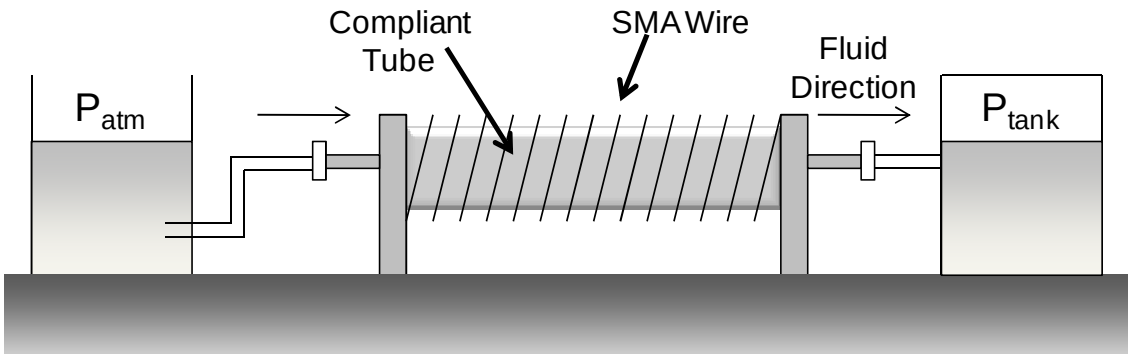

Figure 3.3 Peristaltic pump demonstrating concept of fluid flow with SMA wire.

conical diaphragm equation (3.1), implying a higher output potential for this pump.

Although the output of this pumping chamber seems promising, there are some drawbacks. After actually having built a prototype modeled after this concept shown in Figure 3.4, it became apparent that it would be difficult to force the tube to return to its original state prior to contraction. A stiffer tube could have been used, but this would have required a stronger actuator. This would pose difficulties for fluid actuation since hotter fluids would be required to cause timely actuation. Electrical actuation could be an alternative, but stronger, thicker wires would require more current input that would most likely exceed the output of most common power supplies.

Another disadvantage of this type of pump is that tubing would be difficult to procure. In order to reach optimal output, the diameter needs to be on the order of 5 to 10 cm minimum. Tubing with such diameters is common, but the stiffness of these tubes is so high that the actuator would not cause significant contraction, thus yielding a very low output performance.

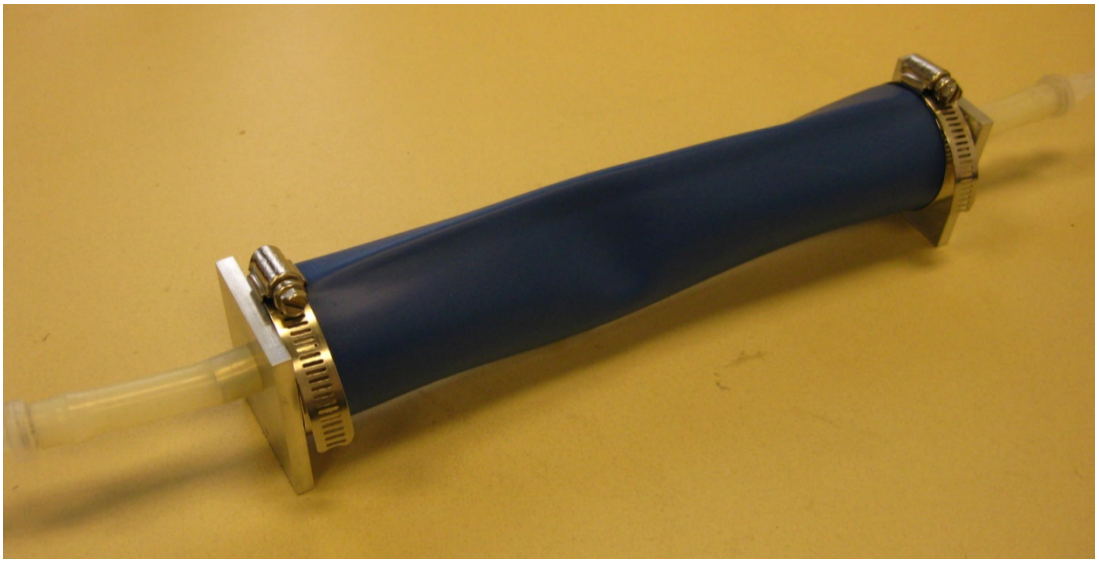

Figure 3.4 Photograph of the peristaltic bladder pump prototype.

3.1.3 Dual Bellows Concept

The final pumping chamber that will be discussed in this thesis is the dual bellows concept. While the concept is similar to the piston-cylinder, there are some output advantages that will be discussed. The overall scheme is shown in Figure 3.5. In this diagram, there is a center plate and on each side is a bellows chamber. Attached to the bellows chambers are plate with two holes – one for inflow and one for outflow. Attached to these holes are tubes with check valves to ensure unidirectional flow. Similar to the piston-cylinder concept, the chambers must pump 180° out of phase.

One item that is not present in this concept is the lever. Instead, the outside plates are attached to the center plate via four SMA actuators each. Since the diameter of the can be much larger, smaller actuators can be used to still achieve high outputs. Due to the increased area within the bellows, additional actuators are required to enable the pump to be able to provide higher pressure inside the pumping chamber to overcome the accumulator pressures in order to pump fluid back into the accumulators.

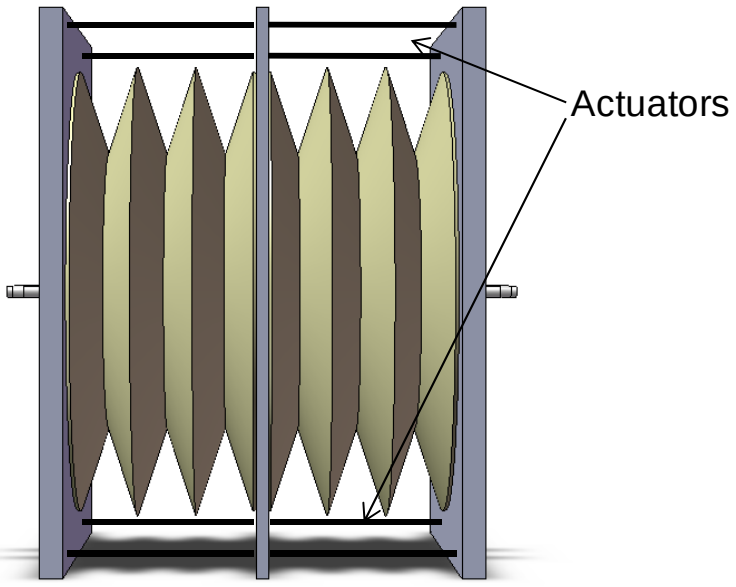

Figure 3.5 Dual bellows concept using four SMA actuators per bellows chamber.

The output of this design is derived directly from that of a typical piston-cylinder. The output per strain is

$$\delta V = \frac{\pi}{4} D^2 h \left(\frac{\delta l}{l}\right) \tag{3.3}$$

where h is the stroke and the other variables are the same as the previously proposed pump designs. While this pump can only provide half the output as the peristaltic concept (equation 3.2), the output is still 1.7 times higher than that of the piston diaphragm (equation 3.1).

The primary drawback to this design is that bellows are generally prone to considerable bulging. This bulging would be substantial especially if the bellows were larger. This bulging in the bellows may cause performance output to be on the order of that of the previous concept introduced by Ertel in [13]. Some measures to avoid this are to limit the bellows size or stiffen the bellows material, but this leads to the similar problems as with stiffening the piston diaphragm and peristaltic chamber. Metal bellows exist to alleviate such bugling, but are typically very expensive due to the intricate forming and welding processes [28].

3.1.4 Final Design Selection

After thorough analysis of each aspect of the design, it is now appropriate to discuss the optimal choice for implementation. Of the three chamber concepts, the one with the highest output per actuator strain is the peristaltic chamber. As mentioned previously in section 3.1.2, a prototype of this was actually built. The limitations were readily apparent after experiments indicated that there was no feasible way of forcing the pumping

chamber back to its original state without means of defeating the purpose of the pump such as forcing fluid into the chamber. Further development of this prototype was soon abandoned after such complications.

The dual bellows design was the next best option concerning theoretical output. Unfortunately, the high volume loss in the bellows became too worrisome to bother implementing. Finding bellows of substantial size was difficult and expensive. Some smaller bellows were obtained for experimental evaluation, but the potential for bulging was readily apparent due to the soft silicone materials used.

Finally, the diaphragm design will be analyzed. While demonstrating the lowest output per actuator strain, the advantages outweigh the disadvantages. The benefits of this design are relative ease of modeling implementation, minimal loss of volume output due to bulging, and inexpensive components for building of the prototype. The diaphragm design is the selected design for the prototype and will be used for analysis and discussion for the remainder of this thesis. It should be noted that the human heart is a reciprocating diaphragm pump.

3.2 Actuation Timing

Section 2.3.2 discussed the concept of pumping fluid across the actuators for a time and then allowing the heated stagnant fluid in the actuator tubes to continue inducing actuation. This would increase the overall pumping output while maintaining the same input. The new output-to-input ratio becomes

$$\left(\frac{Q_{out}}{Q_{in}}\right)_{new} = \frac{Q_{out} + \delta Q}{Q_{in}} \tag{3.4}$$

where Q_{out} is the original volume rate output from the pump to the accumulators, Q_{in} is the original volume rate input to the pump's own wet SMA actuators, and δQ is the additional output to the accumulators due to actuation caused by the heated stagnant fluid within the actuators for a period of time.

Consider two opposing wet SMA actuators, actuator A and actuator B, driving two pumping chambers through a lever as shown in Figure 3.6. Hot and cold fluids are alternately passed through these actuators to cause a reciprocating pumping action. Figure 3.7 compares two timing schemes for this pump; it shows how strain would vary over time for actuator A with and without a stagnation period. The modified flow timing contains the stagnant period while the constant flow timing does not. The upper diagram is a sketch of what the expected strain in actuator A would be. The lower diagram, which is in line with the upper, shows which fluid is traveling through each individual actuator.

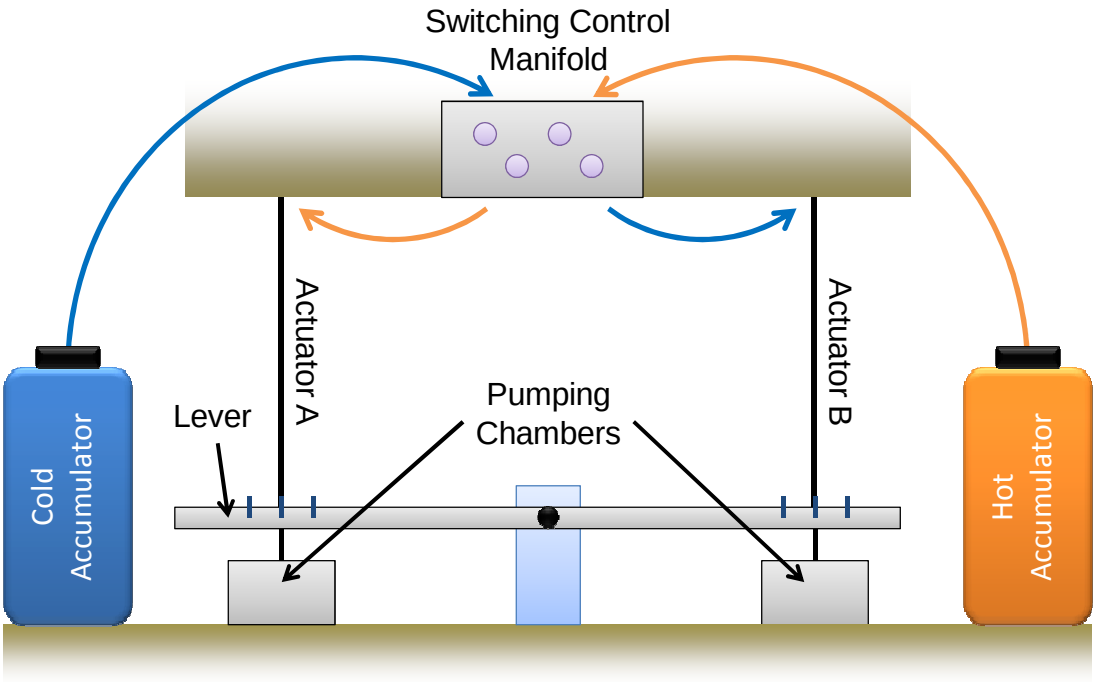

Figure 3.6 Pump schematic of two opposing wet SMA actuators, A and B, causing a reciprocating pump action in the pumping chambers through a lever.

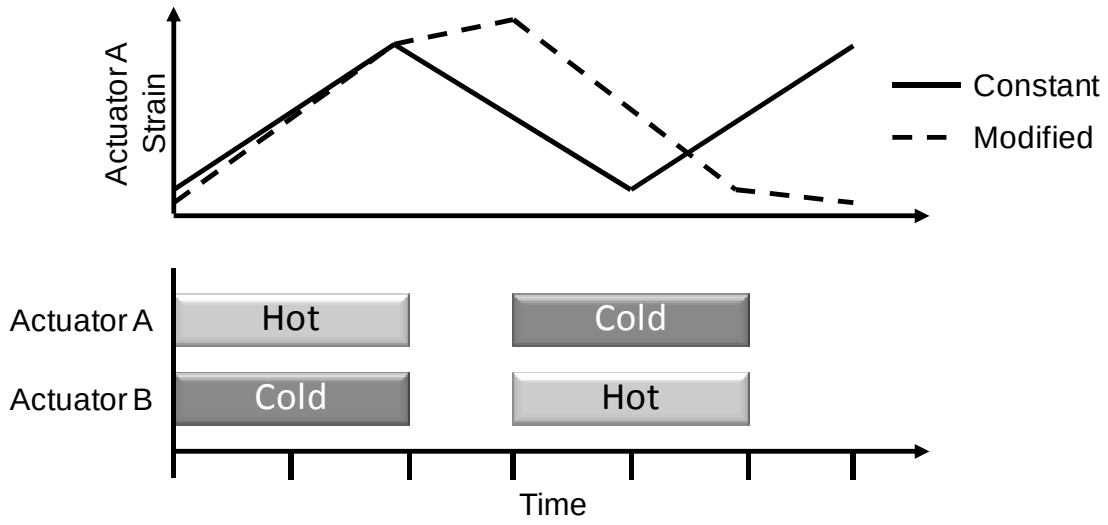

Figure 3.7 Diagram demonstrating actuator strain in line with the thermal fluid phases of the actuators for constant flow and modified flow schemes.

The time between the hot and cold phases is be called the stagnation phase. During this stagnation phase, the strain is still changing, thus increasing the overall output of the pump system. With this increase in output, the output-to-input performance is expected to improve.

3.3 Alternative Working Fluid Analysis

The effectiveness of heat transfer from a fluid to the SMA wire in the actuators is dependent upon multiple factors. Some of these factors are the fluid properties. Many fluid properties affect the heat transfer from the fluid to the wire, but some are more significant and have more of an effect than others. One of these properties is the thermal conductivity of the fluid, k_f.

The rate of temperature change in the wire due to a surrounding fluid is given by

$$\frac{\partial T_{w,f}}{\partial t} = \frac{4D_w k_f Nu_w(x)(T_f - T_w)}{c_{p,w}\rho_w\left(D_f - D_w\right)(D_f^2 - D_w^2)}. \tag{3.5}$$

In equation 3.5, D_w is the SMA wire diameter and D_f is the inner tube diameter; $Nu_w(x)$ is the Nusselt number along the length of the wire; T_f and T_w are the fluid and wire temperatures, respectively; and $c_{p,w}$ and ρ_w are the specific heat and density of the SMA wire, respectively. From this equation, it is evident that in order for faster heat transfer, and thus faster actuation to occur, a high thermal conductivity is desired.

Other desired fluidic properties are low viscosity and high boiling point. Low fluid viscosity allows for lower accumulator pressures. This is desirable since the pumping chambers driven by the actuators need to pump against the accumulator pressure. It is advantageous to minimize this opposing force to increase pump output. A fluid with a higher boiling point is advantageous because it allows for hotter fluid to be passed along the SMA wires. This improves strain in the actuators because there is a more complete phase transformation to austenite.

Figure 3.8 compares the martensite fraction, Rm, of a NiTi wire where the maximum temperature varies from 80°C to 100°C. The martensite fraction is sensitive to the temperature in this range. For this reason alone, using a fluid with a boiling point above 100°C is critical to the performance of the pump. The boiling point of water is depressed at higher elevations, as shown by the solid line in Figure 3.9 [29]. However, it is possible to take advantage of the pressurized conditions within the accumulator. By heating the water within the accumulator, which is typically pressurized to 15 kPa above atmospheric pressure, the boiling point would increase as given by the dotted line in the figure.

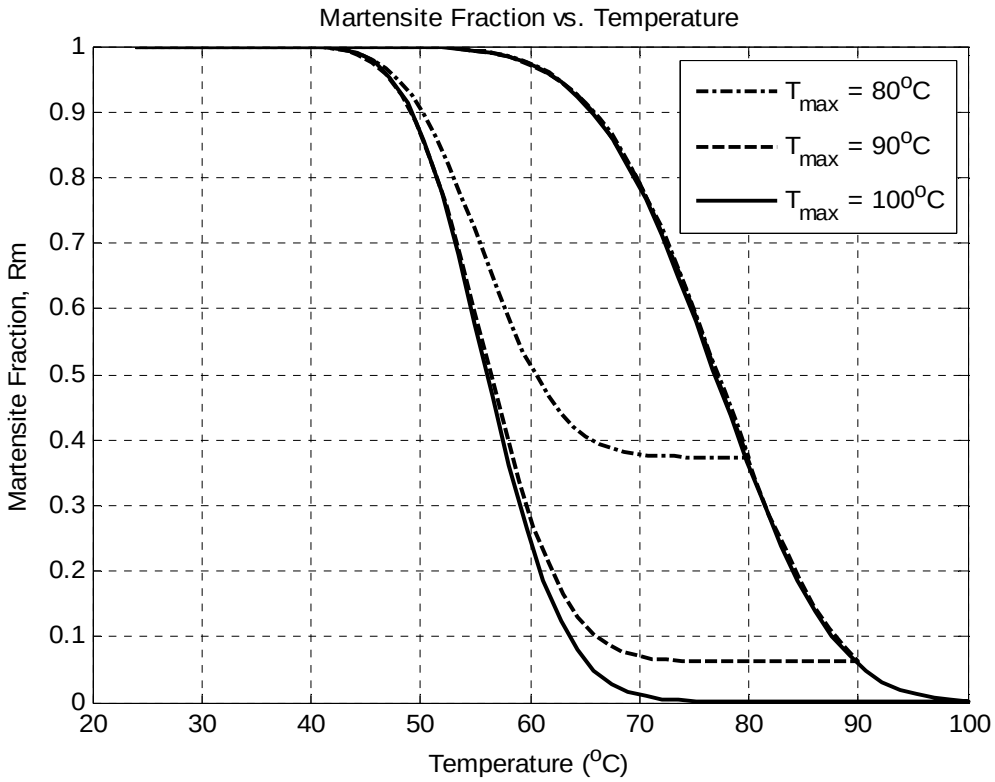

Figure 3.8 Martensite fraction temperature profiles for maximum temperatures of 80°C, 90°C, and 100°C.

Table 3.1 presents the values of these desired properties for water, glycerol, and ethylene glycol at 0.7 atm. Early tests with glycerol and ethylene glycol suggest that high accumulator pressures are required to overcome the fluidic resistance due to high viscosity. Even in mixtures with water, the accumulator pressures required to pump the fluids through the actuators overpowers the actuators' pull strength. Figure 3.10 shows the boiling point of this water-glycerol mixture based on percent weight of glycerol at one atmosphere of pressure [30]. In the interest of exploring the effects electrical actuation, other fluids were not explored. The use of electrical actuation may be used for completing the phase transformation for increased strain and pump performance.

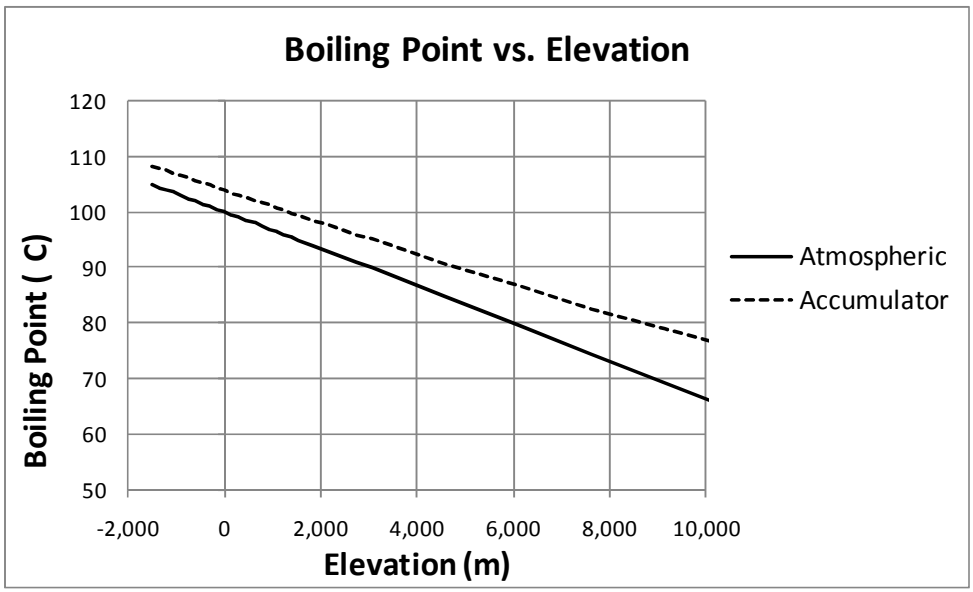

Figure 3.9 Boiling point of water with respect to elevation for atmospheric and 15 kPa accumulator conditions.

Table 3.1 Comparison of desired fluidic properties between water, glycerol, and ethylene glycol at 0.7 atm.

Fluid	Thermal Conductivity (W/m·K)	Viscosity (10^{-4} Pa·s)	Heat Capacitance (J/kg·K)	Boiling Point (°C)
Water	0.643	5.5	4200	92
Glycerol	0.292	30	3138	290
Ethylene Glycol	0.258	150	3210	195

3.4 Electrical Actuation

In addition to using fluidic actuation, electricity can be used to improve the overall output performance of the pump. By using the fluid to perform a significant portion of the actuation, electricity can be used to finish the phase transformation necessary to reach maximum strain. This process can reduce the overall fluid input to the actuators, thus increasing the output-to-input ratio. The drawback to using electrical actuation, or Joule heating, is that an external power supply is needed. Supplying electrical power to the

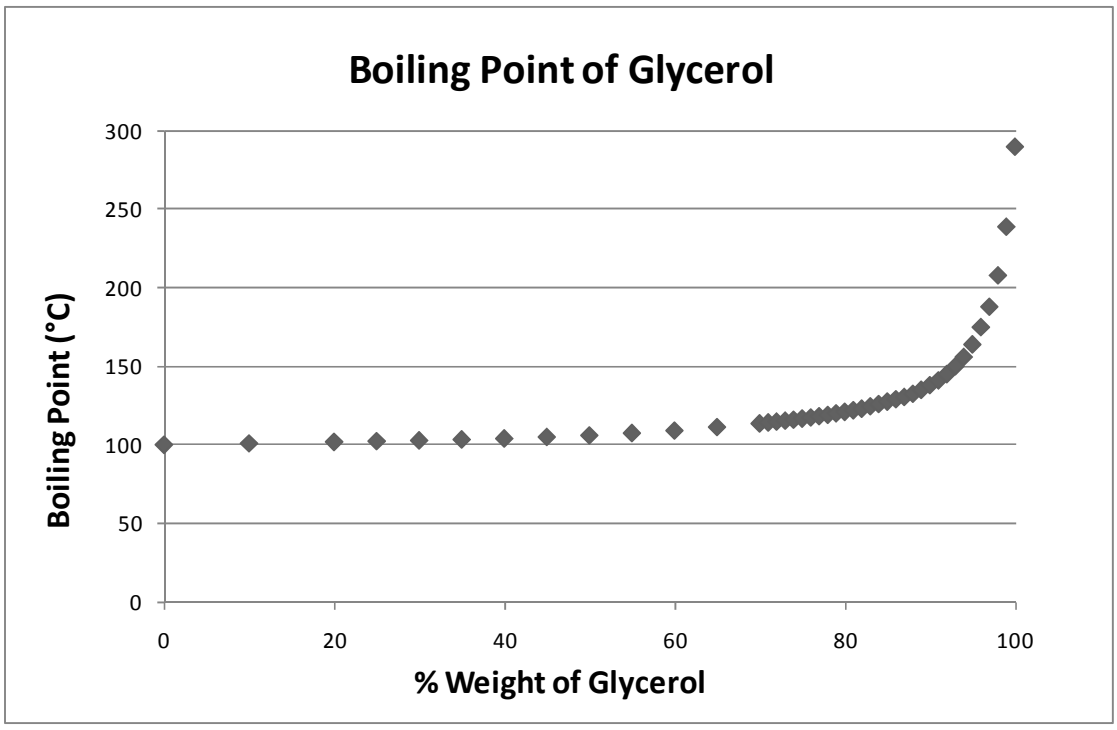

Figure 3.10 Boiling point of glycerol as a function of percentage weight in a water mixture.

SMA actuators also is highly inefficient compared to convection induced actuation [13]. This will reduce the overall energy efficiency of the pump. Section 4.3.4 will discuss the modeling of electrical actuation and its affect on the pump output.

3.5 Heat Loss Minimization

As discussed in section 2.3.4, it is necessary to minimize the heat loss in all areas of the pump. It is of utmost importance to minimize the heat loss from the fluid to the environment as the fluid travels from the accumulators to the actuators. This ensures that the actuators are not being heated by a fluid that is colder than expected and decreases the overall required energy input to the system.

It can be shown that the heat loss rate from the water to the environment through a

long tube at steady-state [31] is given by

$$q_r = \frac{2\pi Lk(T_f - T_a)}{\ln (r_t/r_f)} \tag{3.6}$$

where q_r is the heat transfer rate in the radial direction, L is the tube length, k is the thermal conductivity of the tube, T_f if the fluid temperature, T_a is the ambient temperature, and r_t and r_f are the outer and inner diameters of the tube, respectively. From equation 3.6 it is evident that decreasing the tube length will decrease the heat loss rate. It is also evident that the ratio of the outer and inner diameters of the tube plays a significant role. Holding the inner diameter constant and increasing the outer diameter will decrease the heat loss. Similarly, adding insulation to the tubing would also decrease the heat loss by using a material with a low thermal conductivity.

3.6 Sustaining Output Performance

As mentioned in section 2.1, it is necessary for heat to be continuously added to the system in order to maintain the performance over an extended period of time. There are multiple ways of achieving this. One way would be to heat the fluid inside the tubes prior to it passing along the SMA actuators. This would be difficult since a heating element would need to be placed inside a small diameter. Another way would be to add heat to the water inside the accumulator containing the hot fluid. This option is favorable since it would be relatively simple to place a heating element inside the accumulator while the pump is operating.

3.6.1 Continuous Fluid Heating

Since the efficiency of the pump is one element of concern, the power required to maintain the fluid temperature will now be discussed. Figure 3.11 shows an open thermodynamic system where fluid is allowed to enter and exit at different temperatures. Heat can be added and can also escape the accumulator. Since heat will only be added to the hot water accumulator, the cold water accumulator will not be discussed. By applying the first law of thermodynamics to the system, the total power required to maintain the fluid at a certain temperature is given by

$$q_{in} = -mc_p \frac{\partial T}{\partial t} + \dot{m}_{in}(h_{out} - h_{in}) \tag{3.7}$$

where q_{in} is the power input required, m is the mass of water in the accumulator, c_p is the

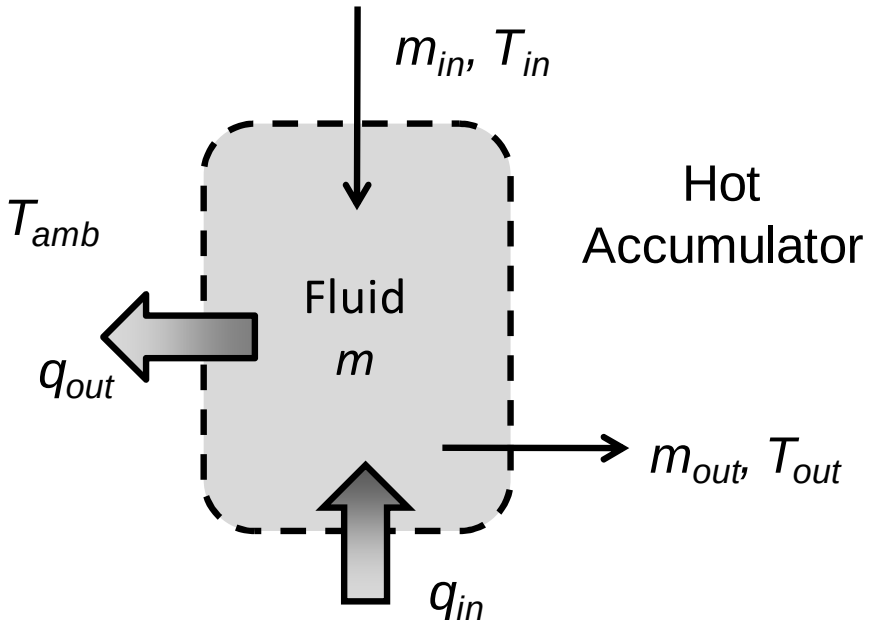

Figure 3.11 Open thermodynamic system of the hot accumulator for deriving the required heat input to maintain pump performance.

specific heat of the fluid, $\frac{\partial T}{\partial t}$ is the instantaneous rate of temperature change due to heat loss within the hot accumulator, $\dot{m}_{in}$ is the mass flow rate into the accumulator, and h_{in} and h_{out} are the enthalpies of the fluid flow in and flow out, respectively. If the hot accumulator is well insulated, the heat loss term can be neglected. It should also be noted that the modified flow control is a nonsteady flow process so the power calculation only applies during periods when fluid is actually flowing. Higher $\dot{m}_{in}$ corresponds to higher output of the pump which, in turn, signifies increased power consumption required to maintain performance.

Although there are an infinite number of possible operating conditions, there are typical sets of operating conditions that can be used to estimate the power input to the system. Consider Table 3.2 for one of these sets of conditions containing values obtained from [32]. The temperature gradient was determined experimentally. Under these conditions it can be determined that the power input will be approximately 275 Watts for an output-to-input ratio of 1.0. By adding insulation to the hot accumulator and neglecting heat loss, the power input reduces by 16% to 230 Watts under the same conditions. For a system where the pump output is higher than the input, the power input will increase significantly in order to heat the additional cooled fluid entering the hot water accumulator. The overall power requirements will also increase with the inclusion of electrical actuation.

The net power efficiency of the pump is given by

$$\eta_P = \frac{P_{accum}(Q_{out} - Q_{in})}{q_{in}} \tag{3.8}$$

Table 3.2 List of typical parameter values for power input calculations.

Symbol	Parameter	Value	Units
-	Fluid	Water	-
m	Fluid Mass	0.5	kg
c_p	Specific Heat	4210	J/kg·K
$\frac{\partial T}{\partial t}$	Temperature Gradient	-0.021	°C/s
$\dot{m}_{in}$	Mass Flow Rate In	0.001	kg/s
$\dot{m}_{out}$	Mass Flow Rate Out	0.001	kg/s
h_{in}	Enthalpy In	146.64	kJ/kg
h_{out}	Enthalpy Out	377.04	kJ/kg

where P_{accum} is the accumulator pressure, Q_{out} and Q_{in} are the volume flow rate output and input of the pump, respectively, and q_{in} is the power input to the pump. By calculating the efficiency of the pump, more efficient configurations can be determined to optimize the pump's performance. For example, electrical actuation may require more power input, but may also lead to a more overall efficient pump due to increased pump output.

Another parameter of interest is the pump's power density, which can be expressed in terms of mass or volume of the pumping apparatus. This mass power density is given by

$$p_m = \frac{P_{accum}(Q_{out} - Q_{in})}{m_P} \tag{3.9}$$

where p_m is the mass power density and m_P is the mass of the pump. The volume power density is expressed as

$$p_V = \frac{P_{accum}(Q_{out} - Q_{in})}{V_P} \tag{3.10}$$

where p_V is the volume power density and V_P is the volume of the pumping apparatus. These parameters are valuable in comparing pump outputs to one another. Generally, pumps with higher power densities are desired as this indicates the power output of a pump with respect to the pump's own physical characteristics which could be a design parameter.

Since the pump will be recycling the fluid used for actuation, it is desired that the hotter and colder fluids are separated such that they are pumped back into their respective accumulators. This will reduce the overall power input required to maintain the hot fluid at a high temperature and will also eliminate the need for supplemental cooling of the cold accumulator due to natural cooling to the environment so long as the colder fluid remains below 40°C as suggested by Figure 3.8. This can be accomplished using solenoid valves to route the fluids at appropriate times during the pumping cycle. Determining this timing can be done with thermocouple feedback or with knowledge of the fluidic flow rate and length of the tubing.

3.7 Conclusions

Due to the considerable amount of improvements that have been suggested in this chapter, it is expected that the overall output-to-input ratio of the pump will be improved dramatically over that of the previous design. The end goal of this thesis is to reach a performance level where significantly more fluid is being pumped than consumed. The next chapter will discuss the modeling results based on these design improvements.

CHAPTER 4

OPTIMIZATION BY MODELING AND SIMULATION

It is beneficial to model the SMA pump dynamics in order to predict the behavior of the system under various conditions. This helps alleviate the number of experiments required in order to find the set of parameters that yields optimal output performance. In order to model the entire pump system, dynamic models of both the SMA actuators and the rest of the system are required. The dynamic model derived by Ertel's [13, 14] work will be used as a starting point for the model used in this thesis.

4.1 Review of the SMA Pump Dynamic Model

Ertel's dynamic model was derived using energy bond graphs and state-space methods. This allowed for combining the individual wet SMA actuator models with the pumping system model. Figure 4.1 shows the complete bond graph used to derive the state equations. In this figure, the actuators are divided into three segments per actuator as opposed to twenty segments used in the actual model. This bond graph couples two opposing actuators each of which are attached to its own pumping chamber through a lever with a given mechanical advantage. The effort sources, S_e, are martensite fractions modulated by SMA wire temperature. These temperatures, determined by simulation of hot and cold water passing through the wet SMA actuators, will now be discussed.

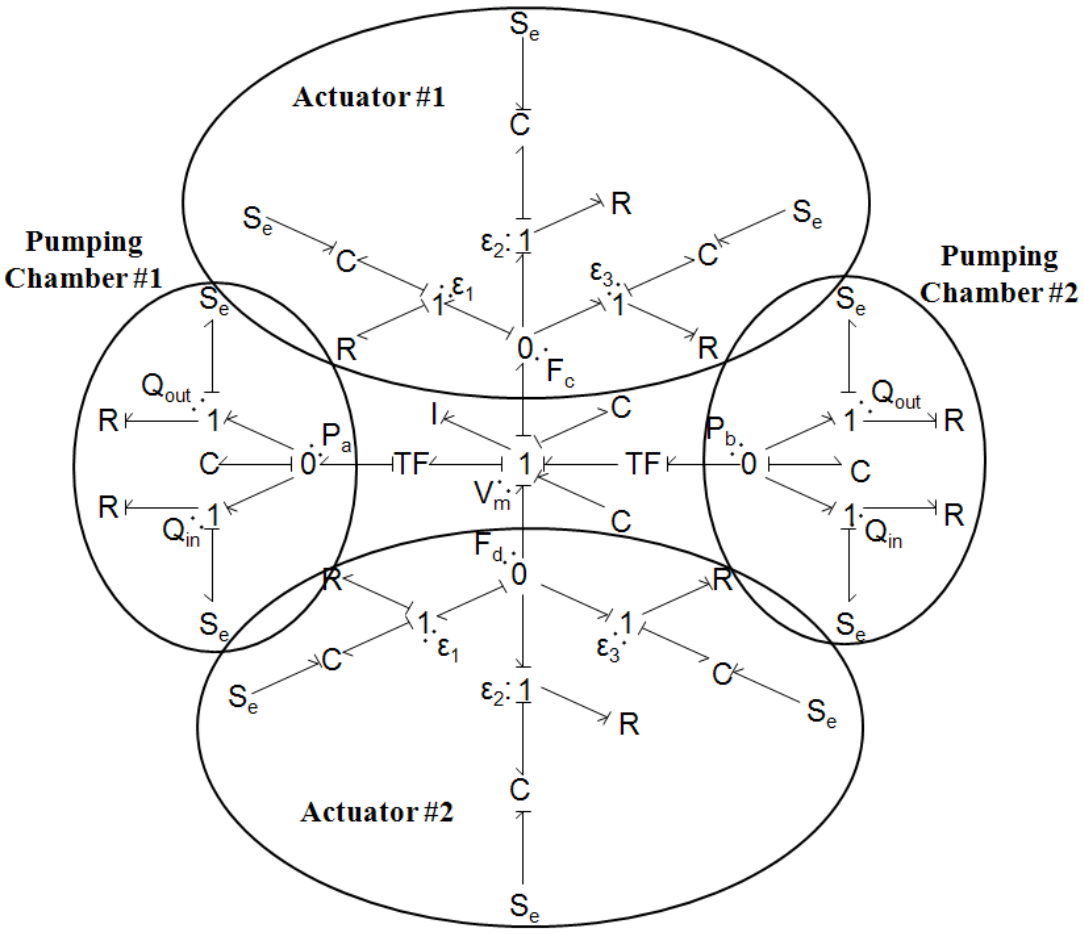

Figure 4.1 Bond graph of the entire SMA pumping system consisting of two wet SMA actuators and two pumping chambers for hot and cold fluid.

By establishing the inlet temperature of the hot and cold fluid into the wet SMA actuators, the temperature rate of change of the fluid along the length of the actuator is given by

$$\frac{\partial T_f}{\partial t} = \frac{T_w - T_f}{\tau_{f,w}(x)} + \frac{T_t - T_f}{\tau_{f,t}(x)} - u_f \frac{\partial T_f}{\partial x} \tag{4.1}$$

where T_f is the fluid temperature, T_w is the wire temperature, T_t is the compliant tube temperature, u_f is the fluid velocity, and x is the length along the actuator. The time

constants in the denominators are given by

$$\tau_{f,w}(x) = \frac{c_{p,f}\rho_f\left(D_f - D_w\right)\left(D_f^2 - D_w^2\right)}{4D_w k_f Nu_w(x)} \tag{4.2}$$

$$\tau_{f,t}(x) = \frac{c_{p,f}\rho_f\left(D_f - D_w\right)\left(D_f^2 - D_w^2\right)}{4D_w k_f Nu_t(x)} \tag{4.3}$$

where $c_{p,f}$ is the specific heat of the fluid, ρ_f is the fluid density, D_f is the inner diameter of the compliant tube, D_w is the diameter of the wire, k_f is the thermal conductivity of the fluid, $Nu_w(x)$ is the Nusselt number between the fluid and the SMA wire, and $Nu_t(x)$ is the Nusselt number between the fluid and the inner surface of the compliant tube. The Nusselt numbers are determined experimentally.

By obtaining the temperature of the fluid along the actuator, it is now possible to calculate the heat transfer from the fluid to the compliant tube and to the SMA wire. The temperature rate of change of the compliant tube is given by

$$\frac{\partial T_t}{\partial t} = \frac{T_f - T_t}{\tau_{t,f}(x)} + \frac{T_a - T_t}{\tau_{t,a}} \tag{4.4}$$

where T_a is the ambient temperature surrounding the actuators. The thermal time constants are

$$\tau_{t,f}(x) = \frac{c_{p,t}\rho_t\left(D_f - D_w\right)\left(D_t^2 - D_f^2\right)}{4D_f k_f Nu_t(x)} \tag{4.5}$$

$$\tau_{t,a} = \frac{c_{p,f}\rho_t\left(D_t^2 - D_f^2\right)}{4k_a Nu_a} \tag{4.6}$$

where $c_{p,t}$ is the specific heat of the tube, ρ_t is the density of the tube, D_t is the outer diameter of the tube, k_a is the thermal conductivity of air, and Nu_a is the Nusslet number between the tube and the ambient air. The rate of temperate change of the SMA wire within the actuator is given by

$$\frac{\partial T_w}{\partial t} = \frac{T_f - T_w}{\tau_{w,f}(x)} \tag{4.7}$$

and the time constant is

$$\tau_{w,f}(x) = \frac{c_{p,w}\rho_w D_w\left(D_f - D_w\right)}{4k_f Nu_w(x)}. \tag{4.8}$$

Upon calculating the temperatures of the components within the wet SMA actuators, the martensite fractions can then be determined along the lengths of the SMA wires. Due to the nonlinear behavior of martensite fraction and temperature, a hysteresis model needs to be applied. As described in [33], the hysteresis can be approximated with a cumulative normal distribution curve. The martensite fraction, R_m, can be expressed as

$$R_m(x) = \frac{1}{2}\left[1 - erf\left(\frac{T_w(x) - \bar{T}}{\sigma_T\sqrt{2}}\right)\right] \tag{4.9}$$

where $\bar{T}$ is the average transformation temperature and σ_T is the standard deviation of the

transformation temperature. These values differ depending on whether the transformation is from martensite to austenite or vice versa and are used accordingly in the model as given by the SMA manufacturer's specifications. Other methods have been used to model this same phase hysteresis [34, 35], but this method has proved to be reliable based on Ertel's application and results.

Before listing the dynamic states of the model, it is still necessary to mention other modulating variables such as strain and stress within the SMA wire of the actuators as they are influenced by the phase transformation. Noting that the actuators are divided into segments, the strain of each of the SMA wire segments is given by

$$\epsilon = \begin{cases} \dfrac{4F/\pi D_w^2}{E_a + R_m(E_m - E_a)}, & \epsilon \le \epsilon_m^y \\ \dfrac{4F/\pi D_w^2 - R_m\epsilon_m^y(E_m - E_t)}{E_a + R_m(E_t - E_a)}, & \epsilon_m^y < \epsilon \le \epsilon_m^d \\ \dfrac{4F/\pi D_w^2 - R_m\left[\epsilon_m^y(E_m - E_t) + \epsilon_m^d(E_t - E_d)\right]}{E_a + R_m(E_d - E_a)}, & \epsilon > \epsilon_m^d \end{cases} \tag{4.10}$$

where ϵ is the strain, ϵ_m^y is the yield strain of fully twinned martensite, ϵ_m^d is the minimum strain of detwinned martensite, F is the force in the actuator segment, and E_a, E_m, E_t, and E_d are the moduli of elasticity for austenite, martensite, twinned and detwinned martensite, respectively. By calculating the strain, the stress, σ, can be expressed as

$$\sigma = \begin{cases} E_m\epsilon, & \epsilon \le \epsilon_m^y \\ E_m\epsilon_m^y + E_t\left(\epsilon - \epsilon_m^y\right), & \epsilon_m^y < \epsilon \le \epsilon_m^d \\ E_m\epsilon_m^y + E_t\left(\epsilon_m^d - \epsilon_m^y\right) + E_d(\epsilon - \epsilon_m^d), & \epsilon > \epsilon_m^d \end{cases} \tag{4.11}$$

and used to calculate the force in the actuators.

With all of the modulating variables now accounted for, the states of the model will now be presented. The states include actuator force, stress and strain, piston position and velocity, pumping chamber pressure, and volume output. The force state equation is

$$\dot{F} = \frac{\pi}{4} D_w^2 \left[E_a (1 - R_m) \dot{\epsilon} - E_a \dot{R}_m \epsilon + R_m \dot{\sigma} + \dot{R}_m \sigma \right]. \tag{4.12}$$

The state equations for $\dot{\epsilon}$ and $\dot{\sigma}$ are

$$\dot{\epsilon}_i = \frac{1}{R} \left[\frac{1}{n} \left(\sum_{j=1}^{n} F_j + \frac{R}{\Delta L} V_m \right) - F_i \right] \tag{4.13}$$

$$\dot{\sigma} = \begin{cases} E_m \dot{\epsilon}, & \epsilon \leq \epsilon_m^y \\ E_t \dot{\epsilon}, & \epsilon_m^y < \epsilon \leq \epsilon_m^d \\ E_d \dot{\epsilon}, & \epsilon > \epsilon_m^d \end{cases} \tag{4.14}$$

where R is the linear damping coefficient, n is the number of actuator segments, F_j is the force in each segment force, ΔL is the length of each segment, and V_m is the velocity of the end of the actuators. The state equation for V_m is

$$\dot{V}_m = \frac{1}{m} \left[\frac{A_p}{Ma} (P_{c2} - P_{c1}) + \frac{1}{n} \left(\sum_{j=1}^{n} F_{j,2} - \sum_{j=1}^{n} F_{j,1} - \frac{2R}{\Delta L} V_m \right) \right] \tag{4.15}$$

where A_p is the surface area of the piston, Ma is the mechanical advantage through the lever, and P_{c1} and P_{c2} are the pumping chamber pressures.

The state equations for the two pumping chambers are expressed as

$$\dot{P}_{c1} = \frac{1}{C}\left[\frac{A_p}{Ma}V_m - \frac{1}{R_{out}}(P_{c1} - P_{accum}) - \frac{1}{R_{in}}P_{c1}\right] \tag{4.16}$$

$$\dot{P}_{c2} = \frac{1}{C}\left[-\frac{A_p}{Ma}V_m - \frac{1}{R_{out}}(P_{c2} - P_{accum}) - \frac{1}{R_{in}}P_{c2}\right] \tag{4.17}$$

where C is the volumetric capacitance within the piston chambers, P_{accum} is the accumulator pressure, and R_{in} and R_{out} are the fluidic resistances in and out of the pumping chambers. The values of these fluidic resistances approach infinity against check valves.

As mentioned in section 2.2, the results of the model did not exactly match the experimental results. The model was also limited in that it did not allow for complex timing control and electrical actuation. The purpose of this chapter is to explain improvements made to the preexisting model and discuss the effects of the changes made. Plots will be provided as a method of comparison for the two models. The Matlab simulation code is provided in Appendix B.

4.2 Modeling Improvements

Although the results of the previous model were fairly close to the experimental results, there was still room for improvement. One area for improvement was the inclusion of temperature-dependent fluid parameters. It is known that water parameters such as viscosity, heat capacity, and thermal conductivity vary over temperature. Although some of these parameters may not vary much between 20°C and 100°C, the thermal conductivity varies substantially. As mentioned in section 3.3, the thermal conductivity of a fluid is a major contributor to the efficiency of a fluid causing fast actuation. Figure 4.2 shows the thermal conductivity of water over the working

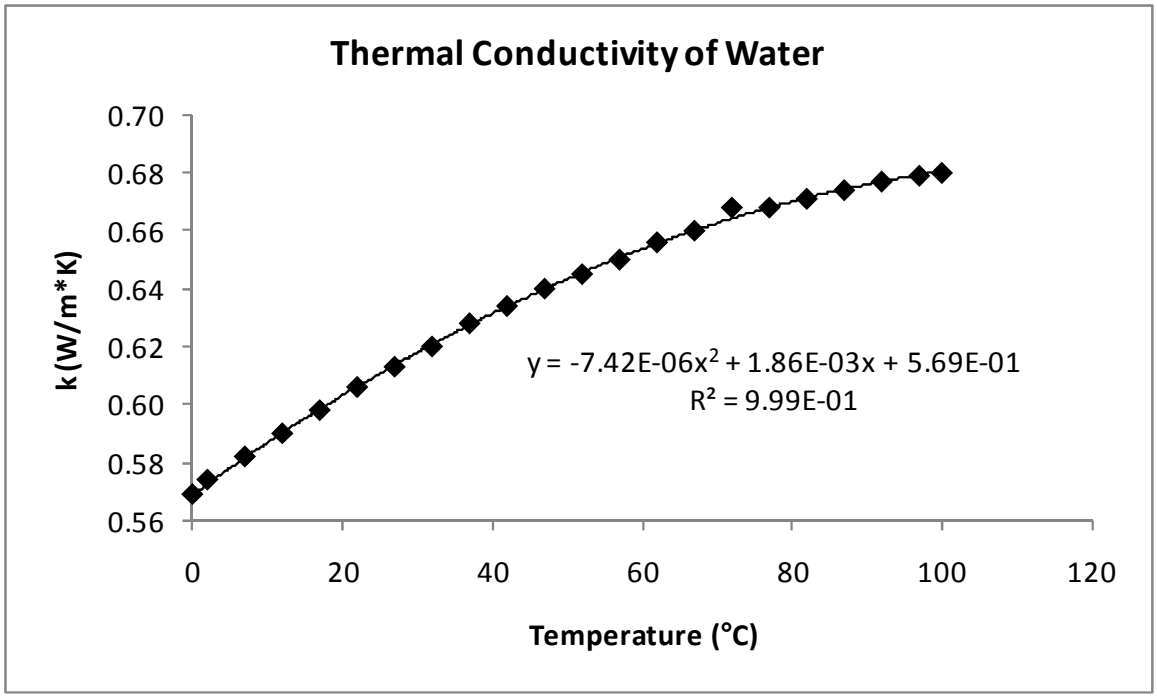

Figure 4.2 Thermal conductivity of water over the working temperature range with a second-order polynomial fit.

temperature range [31]. As is noticeable, the change in the thermal conductivity can vary as much as 20%. These variances can have a measurable effect on the overall model prediction of the output performance. A second-order polynomial fit to this data was used for the pump simulations in sections B.2 and B.3.

Another factor that can be improved in the original model is that of the thermal hysteresis. Ertel [13] mentions using a similar method as provided in [33] to model the hysteresis, but the actual code uses a more simplified method to estimate the martensite fraction based on a linear scaling constant. By modifying the model to the method provided in [33], it can be shown that there is some difference in the overall behavior of the martensite fraction over some specified temperature range. Figure 4.3 shows this difference for the forward and reverse transformations over the temperature range of 20°C to 90°C. “Original” refers to the previous model used in [13] and “Modified” refers

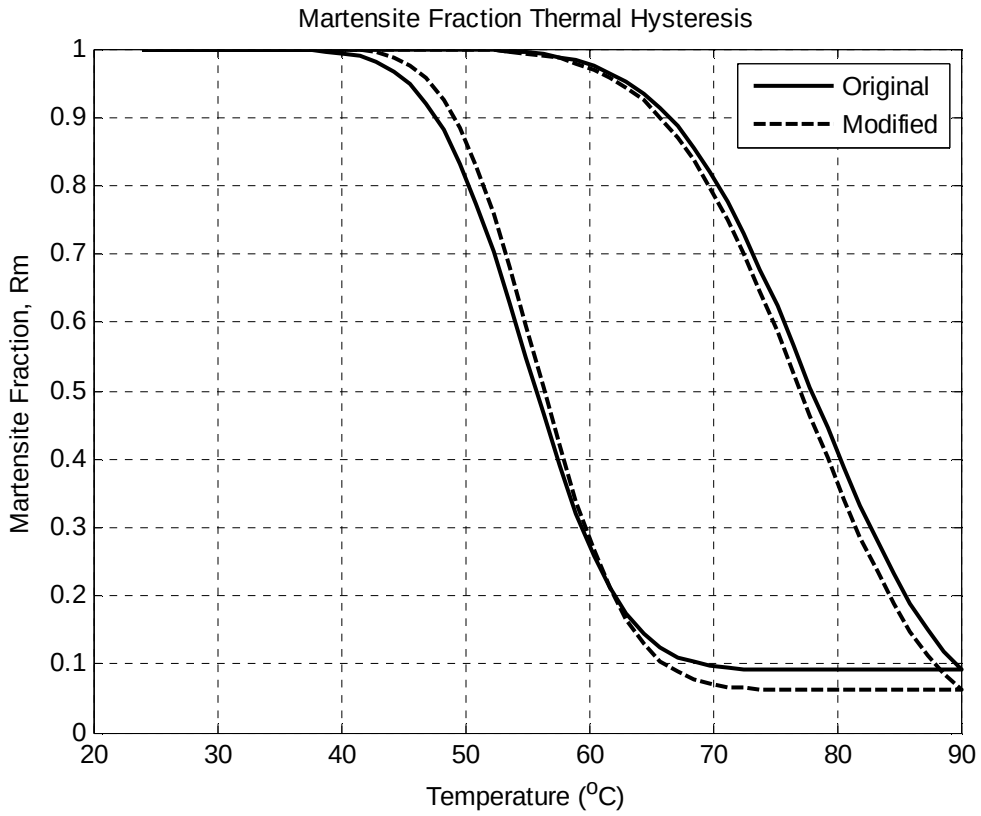

Figure 4.3 Martensite fraction thermal hysteresis comparison of the original and modified models over the temperature range of 20°C to 90°C.

to the method used in this thesis as presented in [33]. With the temperature-dependent properties and the thermal hysteresis correction, the overall output performance prediction varies as much as 20% depending on actuator length, hot water temperature, and accumulator pressure.

As mentioned previously, the original model did not allow for timing control of the fluid. Section 3.2 describes the theoretical changes that would occur if controlled flow of the fluid were allowed. This meant that the fluid would have to be propagated only during a certain time interval and then allowed to be static for a desired duration. Figure 4.4 shows a comparison of the two models using 30 cm actuators and 90°C water. It should be noted that this figure does not show the optimal parameters for the pump since other

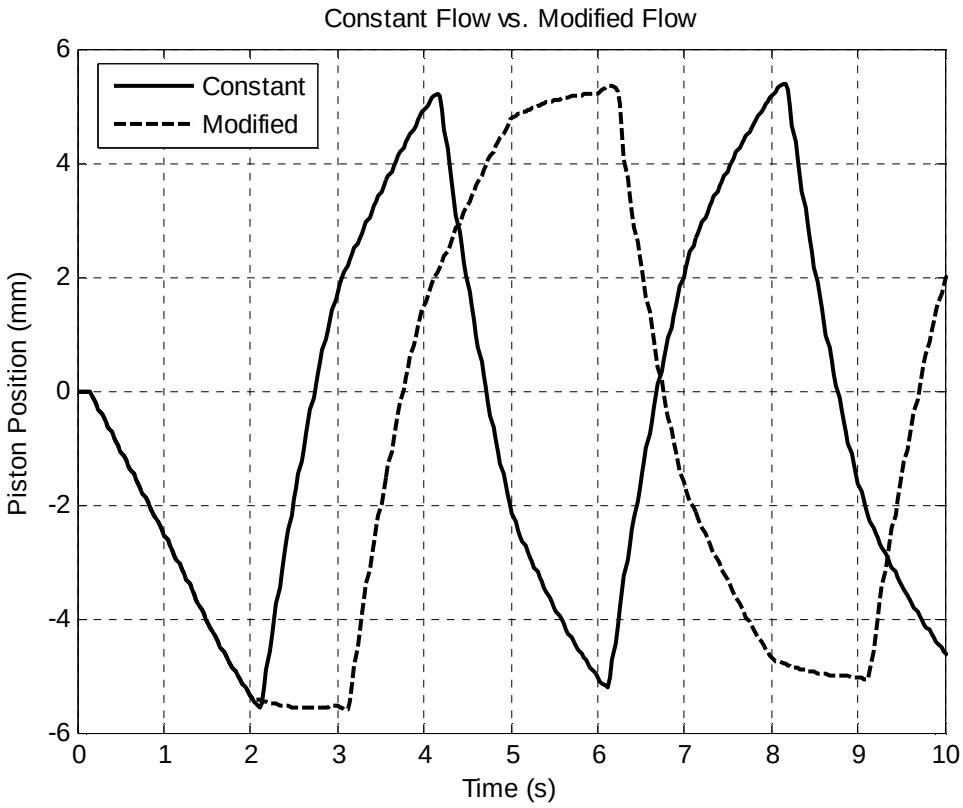

Figure 4.4 Comparison of the original constant flow model with the modified flow model for 30 cm actuators with 90°C hot water.

actuator lengths can be used along with different duration periods. The output-to-input ratio prediction with the constant flow model is 0.203 while the controlled flow model predicts an increase to 0.481. This increase is in agreement with the theoretical increase discussed in section 3.2 where the output is increased while maintaining the same input, thus increasing the output-to-input ratio. The changes made to the Matlab model thus far can be found in section B.2. Actual results are located in section 5.2.

The final improvement to the previous existing model was the incorporation of electrical actuation. By adding electrical heating in addition to the fluidic convection, the overall output of the system can be increased while also potentially lowering the fluid input at the same time. The rate of change in temperature of a SMA actuator is given by

$$\frac{\partial T_w}{\partial t} = \frac{4i^2 R}{\pi D_w^2 \rho_w c_{p,w}} + \frac{\partial T_{w,f}}{\partial t} \tag{4.18}$$

where i is the electrical current, R is the electrical resistance of the SMA wire per unit length of wire, $\partial T_{w,f}/\partial t$ is given in equation 3.5, and the remainder of the terms are defined identically to those in mentioned in sections 3.3 and 4.1. This temperature change is used for modulating the SMA wire martensite fraction and does not affect the bond graph or the state equations.

Figure 4.5 presents a comparison of the piston position for fluid-only actuation and electrical actuation. It should be noted that the electrical actuation still requires some fluid input for additional heating and cooling of the SMA wires inside the actuators. In the figure, hot and cold fluid is passed through the actuators for 2 seconds then electrical actuation occurs for 1 second within the heated actuator to complete the full phase transformation of the SMA wire. The actuator length used in these simulations was 30 cm and the hot water temperature was 90°C. The total output-to-input performance of the fluid-only actuation model was 0.481 while the performance with the electrical actuation increased by almost 75% with an output-to-input ratio of 0.834.

4.3 Model Sensitivity to Design Parameters

In order to effectively test for optimal performance by actual experimentation, it is necessary to find a range for which optimal performance is expected. By varying key parameters and modeling their influence on performance, it is possible to eliminate unnecessary testing that would otherwise produce less useful data. This section will discuss the performance sensitivity to actuator length, mechanical advantage in the

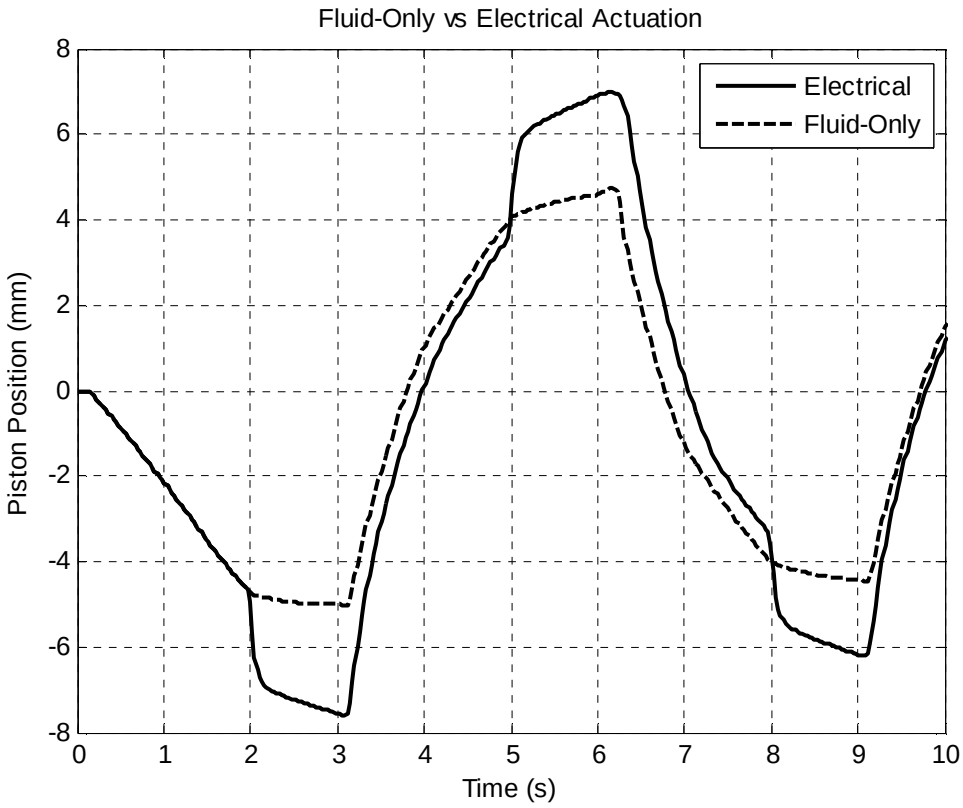

Figure 4.5 Piston position comparison for fluid-only and electrical actuation with 30 cm actuators and 90°C hot water.

pumping lever, actuation timing, water temperature, and electrical actuation. Figures and tables will be provided to demonstrate the performance sensitivity of each parameter.

4.3.1 Actuator Length and Mechanical Advantage

Some of the most key parameters that influence the output performance of the system are actuator length and mechanical advantage. Although having a larger length can be advantageous because larger strain can occur, the downside is that more flow input is required and the heat loss to the environment is increased. Due to this tradeoff, an optimal length is expected for peak performance. Similarly, a high mechanical advantage can be beneficial for overpowering the accumulator pressure, but in a trade for piston

stroke length. By lowering the mechanical advantage and placing the actuator closer to the fulcrum of the lever, the output performance is expected to increase until the force required to move the pistons is greater than the actuator force can supply at which point the performance is expected to decrease.

Figure 4.6 provides simulation results of output-to-input ratio for varying actuator lengths and mechanical advantages (MA). The mechanical advantages shown were chosen based on preliminary indications from the model that smaller values would lead to undesired stress in the actuators and higher values would lead to low output. Flow duration of 4 seconds with a stagnation period of 2 seconds were used for actuation timing over two complete cycles. A hot water temperature of 88°C was used to match the local boiling point and compensate for the heat loss from the accumulator to the

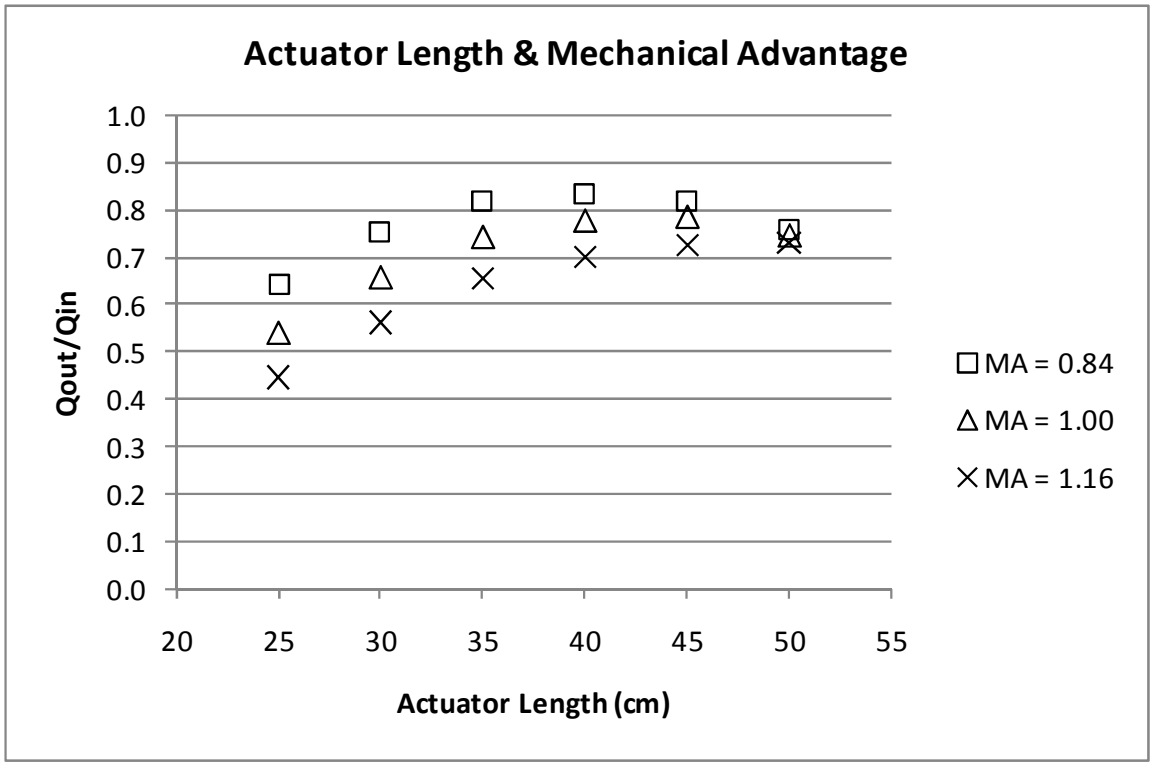

Figure 4.6 Simulation results of output-to-input ratio demonstrating sensitivity to actuator length and mechanical advantage (MA).

actuators. An accumulator pressure of 15 kPa was used to match that which will be used in the actual experiments.

From this plot, it can be deduced that the performance of the pump is expected to reach its maximum potential with actuator lengths between 35 cm and 45 cm. Also, as the mechanical advantage decreases, the output increases for nearly all actuator lengths and then decreases as predicted. Similar results hold true for other timing control schemes including that which allows for stagnant actuation. A mechanical advantage of 0.84 will be used for the remaining simulations in this thesis since modeling suggests that this produces the highest output.

4.3.2 Fluidic Actuation Timing

The timing and control of the fluid passing through the actuators is critical to the performance of the pump. The optimal timing will depend greatly on the actuator length. Longer actuators will require longer flow durations in order to cause full phase transformation along the entire wire within the actuator while smaller actuators will require less. In order to fully understand the relationship between actuator length, flow duration, and output performance, multiple simulations need to be completed.

Figure 4.7 presents the results of 24 simulations of varying actuator lengths and flow durations. The other parameters used are similar to those described in section 4.3.1 for the simulations of actuator length and mechanical advantage. In the figure, it is shown that there exists an optimal flow duration for each actuator length. For example, the optimal flow duration for a 40 cm actuator is 4 seconds and yields a performance ratio of 0.84 which also happens to be the highest predicted performance of the pump using fluid-only actuation. As expected, longer flow durations for smaller actuators results in lower

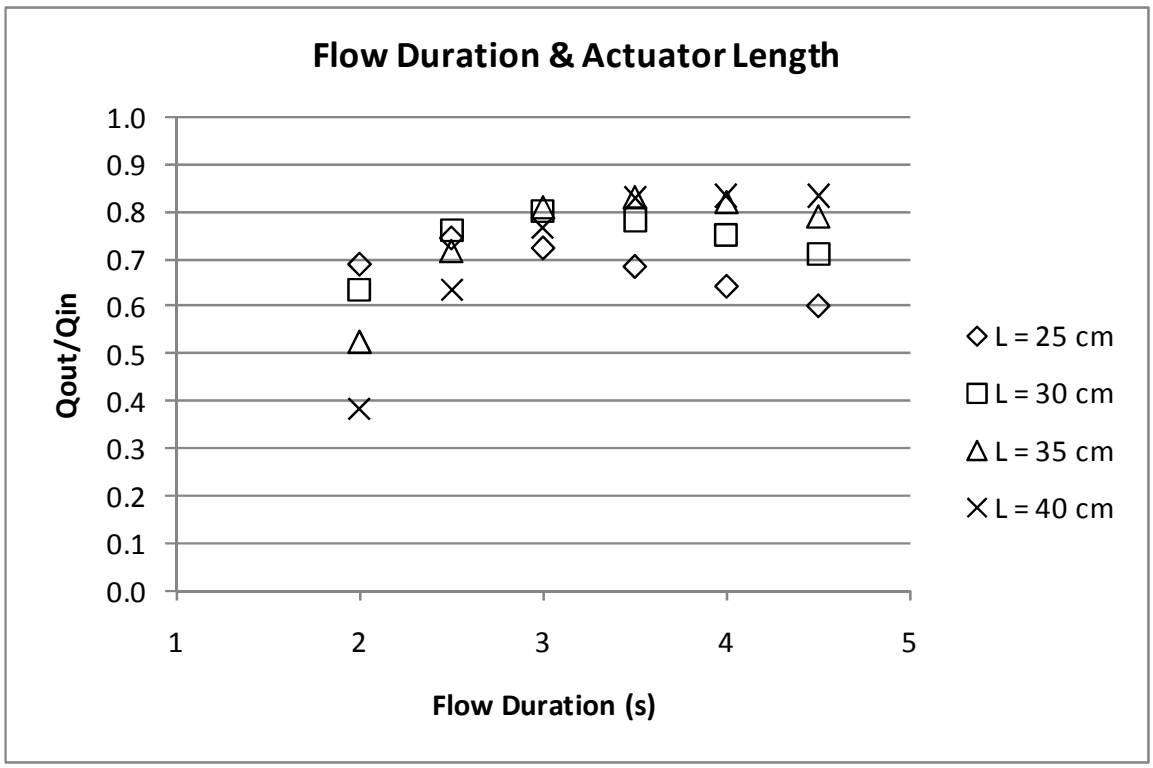

Figure 4.7 Simulation results of output-to-input ratio demonstrating the relationship of flow duration and actuator length.

performance since input flow is being wasted and not inducing significant additional actuation. Conversely, smaller flow durations are not causing enough actuation in longer actuators, thus also reducing the performance. It should be noted that the required fluid propagation time through the actuator is generally less than 1.0 seconds for actuators less than 40cm with an accumulator pressure of 15 kPa.

4.3.3 Fluid Temperature

As mentioned in section 2.3.3, the performance of the pump will vary depending on the temperature of the hotter fluid. Since water is the current working fluid, a simulation analysis of the performance of the pump versus temperature will now be provided. The dependence of the output-to-input ratio performance on hot water temperature within an

effective temperature range for water is provided in Figure 4.8. Similar parameters were used to those mentioned is section 4.3.2 with 40 cm actuators and a flow duration of 4 seconds. As is readily apparent, the performance varies significantly based on the hot water temperature. At sea level where the boiling point is roughly 100°C, the performance is expected to exceed a ratio of 1.0. At higher elevations, this performance ratio may be unreachable without the assistance of electrical actuation or internal accumulator heating as mentioned in section 3.3.

4.3.4 Electrical Actuation

Simulating the electrical actuation as discussed in section 4.2 will provide useful insight to the expected performance increase. Although a performance increase is expected with electrical actuation, there are multiple ways of implementing it. Perhaps

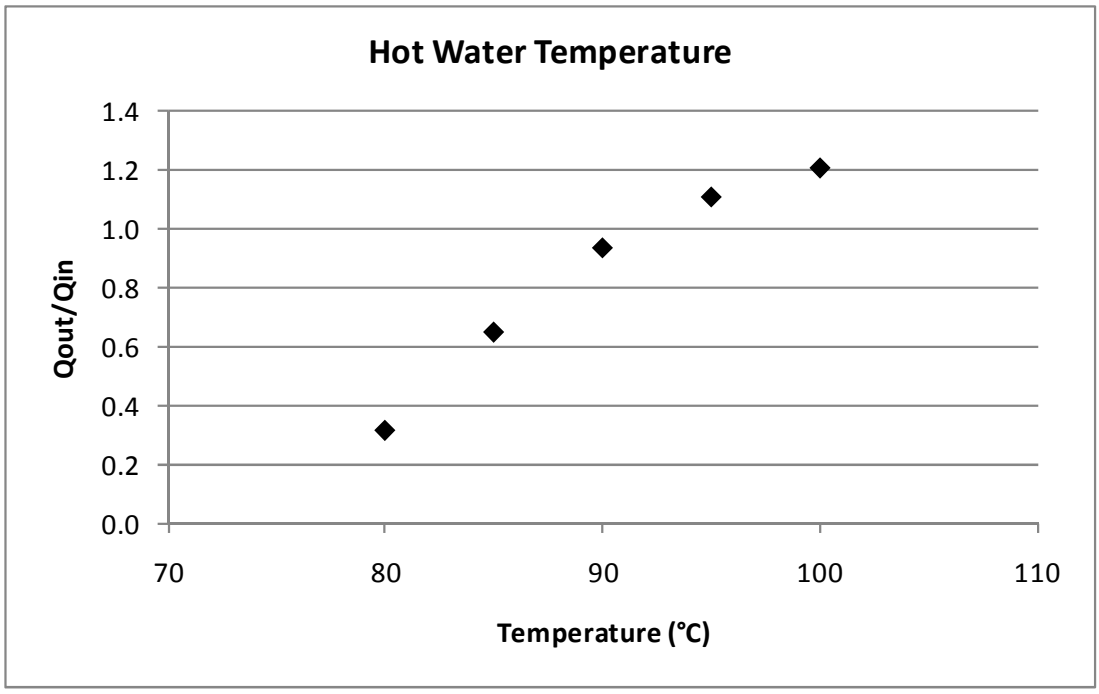

Figure 4.8 Simulation results of output-to-input ratio and the dependence on hot water temperature within an effective range for water.

the simplest way to implement it is to run fluid-only actuation for some duration of time then provide the electrical current to finish the phase transformation. This can be accomplished either during the fluid flow or after. By varying the time at which electrical actuation begins, the optimal timing can be determined via simulation.

Figure 4.9 provides the simulation results for various flow durations and electrical timings. The lead time is defined as the amount of time prior to fluidic flow stopping that the electrical actuation begins. A lead time of 0.0 seconds means that the electrical actuation begins at the time the fluid stops. An electrical duration of 1 second was used for these simulations since prolonged durations of passing current through the actuators can cause permanent deformation. The electrical current used for the simulations was 4.5 Amps. The remaining parameters used reflect those used to obtain the maximum fluid-

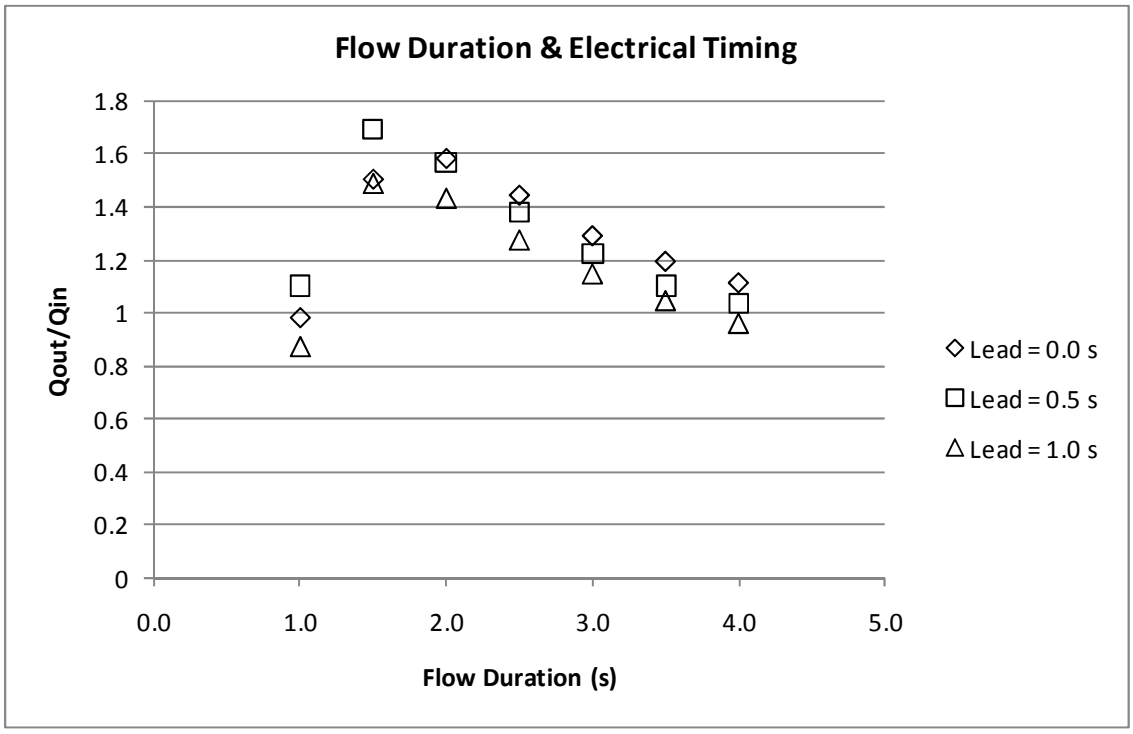

Figure 4.9 Simulation results of output-to-input ratio and various timing schemes of fluid-only flow duration and electrical actuation lead timing.

only performance discussed in section 4.3.2.

The data presented in the figure suggest that a flow duration of 1.5 seconds with 0.5 second lead time yields the highest overall performance. This seems intuitive since additional flow may be unnecessary with the electrical actuation. The data also suggests that there is a point at which flow duration is too small since the fluid propagation time is roughly only 0.8 seconds. This is because the electrical actuation does not provide enough heat to contract the SMA actuators with colder fluid surrounding them. The only way to compensate for this effect would be to increase the amount of current being passed through the SMA actuators. This would require more capable power supplies to accommodate currents above 5 Amps. This topical area will not be covered within this thesis.

4.4 Optimal Design Parameters

Based on simulation results in the previous section, Table 4.1 presents two sets of parameters that will lead to expected maximum; one set for fluid-only actuation and

Table 4.1 List of optimal parameter values for fluid-only and electrical actuation that yields the absolute maximum performance expected for each configuration.

Parameter	Fluid-Only	Electrical	Units
Wire lengths	40	40	cm
Mechanical Advantages	0.84	0.84	-
Accumulator Pressures	15	15	kPa
Hot Water Temperature	88	88	°C
Cold Water Temperature	25	25	°C
Flow Duration	4.0	1.5	sec
Electrical Lead Time	-	0.5	sec
Electrical Duration	-	1.0	sec
Electrical Current	-	4.5	A

another set incorporating electrical actuation. These sets of parameters represent the values used to reach the absolute maximum performances provided in Figure 4.7 and Figure 4.9. It should be noted that the hot water temperatures listed in the table represent that which would be expected during actual experimentation at an elevation of roughly 1400 meters. As mentioned previously, better performance would be obtainable at lower elevations.

4.5 Conclusions

By improving the existing model, implementing electrical actuation, and determining an optimal set of parameters with which the pump will exceed an output-to-input ratio greater than 1.0, it can now be expected that the prototype pump will meet the necessary requirements to be able to supply fluids to external SMA subsystems. The next step is to validate the model by providing actual experimental results and comparing them to the simulation results presented in this chapter. This validation is crucial to being able to continue manipulating the model to find other sets of parameters that could improve the performance of the pump in the future.

CHAPTER 5

PROTOTYPE AND EXPERIMENTAL RESULTS

The previous chapter discussed improvements made to the model and presented the output-to-input results of multiple simulations where key parameters were varied to find an optimal set that would yield maximum performance. Two types of sets were presented: one using fluid-only actuation and the other incorporating the assistance of electrical actuation. This chapter will present the prototype built for testing, provide experimental results for various parameters sets, and compare the pump performance to the simulation results.

5.1 Design Implementation Prototype

In order to compare experimental results with simulation results, a prototype must be built that represents the model in every way possible to ensure the validation of the model is accurate. The prototype must implement the design improvements discussed in Chapter 3 including the new diaphragm design, utilizing complex timing control, electrical actuation, fluid separation and recycling, and continuous heat addition. Figure 5.1 is an actual photograph of the working prototype used for experimental testing. This prototype implements the design improvements just mentioned and allows for parameter variation such as actuator length and mechanical advantage. The design also requires less tubing in

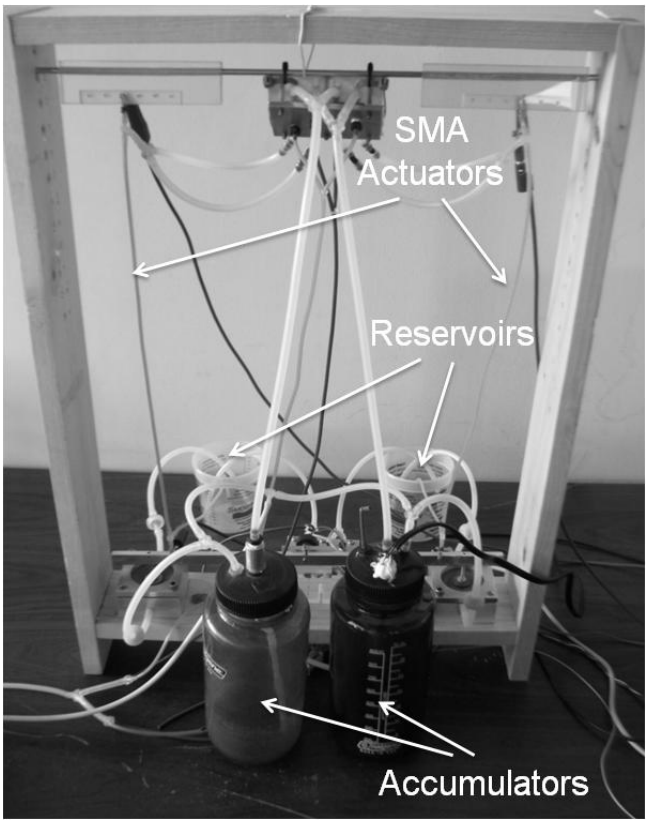

Figure 5.1 Design prototype capable of various wire lengths, mechanical advantages, complex timing, fluid separation, and allows for electrical actuation.

order to minimize heat loss as described in section 3.5. A heating element is located inside the hot water accumulator in order to sustain performance over extended periods of time. The flow path is controlled by four solenoid valves; two control the fluid input to the actuators through a control manifold and the other two separate the hot and cold fluid output from the actuators through a separation manifold. Two power supplies are used to actuate the two individual actuators. Figure 5.2 shows this concept in more detail. A custom LabVIEW program controls the timing of the solenoid valves and the power supplies. A screenshot of the front panel interface is provided in Appendix C.

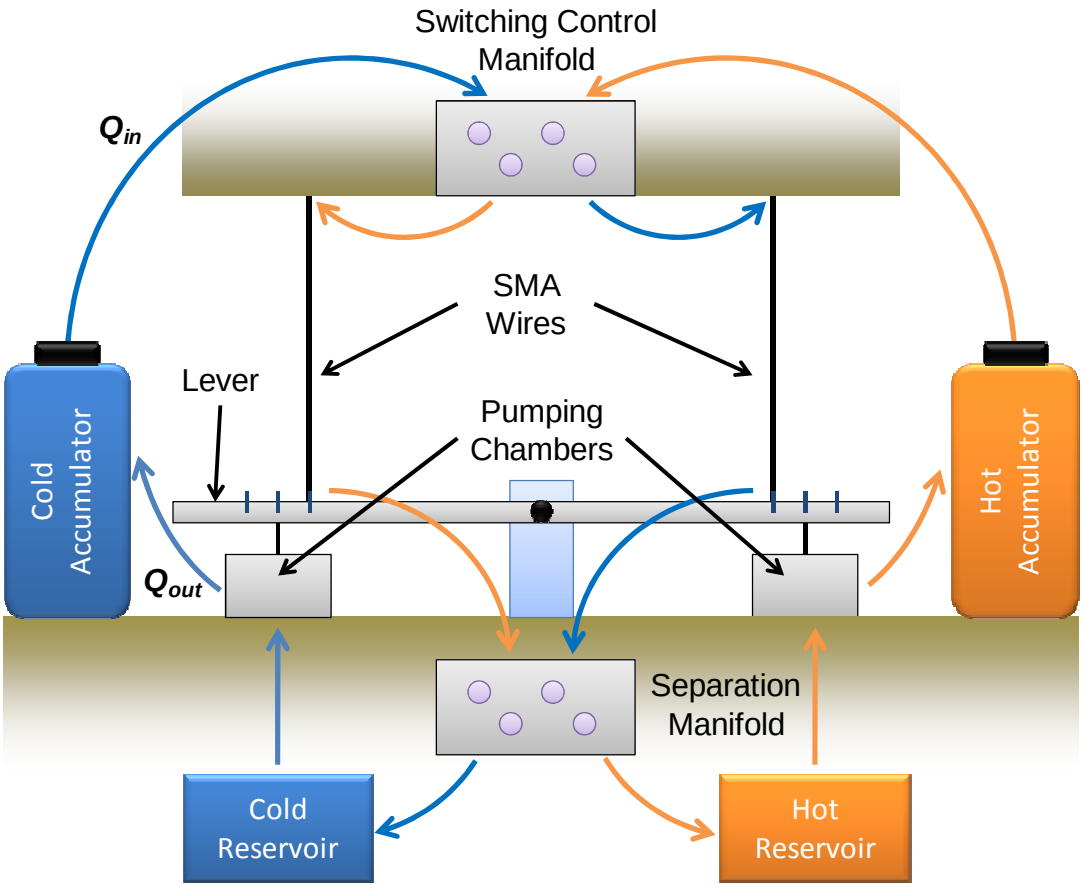

Figure 5.2 Conceptual diagram of the of the new design prototype conveying the flow paths of alternating hot and cold water.

5.2 Experimental Testing and Results

In order to map and obtain optimal performance, a targeted set of experiments were selected to evaluate optimality of the chosen design. First, the optimal flow duration was found for each actuator length by using simulation results as a baseline and then performing quick tests to determine the optimal flow duration by monitoring the output. Upon obtaining the optimal timing for each actuator length, formal fluid-only actuation tests were conducted varying actuator length and mechanical advantage similarly to that described in section 4.3.1. Due to some inconsistency of the pump performance, multiple test runs were performed in order to obtain an average representation for each

configuration.

Figure 5.3 provides the results of the experiments varying actuator length and mechanical advantage. As is evident in the plot, and as predicted in section 4.3.1, the smaller mechanical advantage configurations outperformed those with larger ones. It is also apparent that higher outputs were achieved with longer actuator lengths. This was expected from the simulation results as well. The maximum output-to-input performance obtained with fluid-only actuation under the conditions provided was 0.88. This is almost double that of the previous pump design in [13]. By lowering the accumulator pressure, higher performance was obtained, but this required longer flow duration and was unsuitable for practical application since the pressure could not induce a significant flow that would be useful towards actuating other subsystems.

For fluid-only actuation, the experimental and simulation results are quite similar.

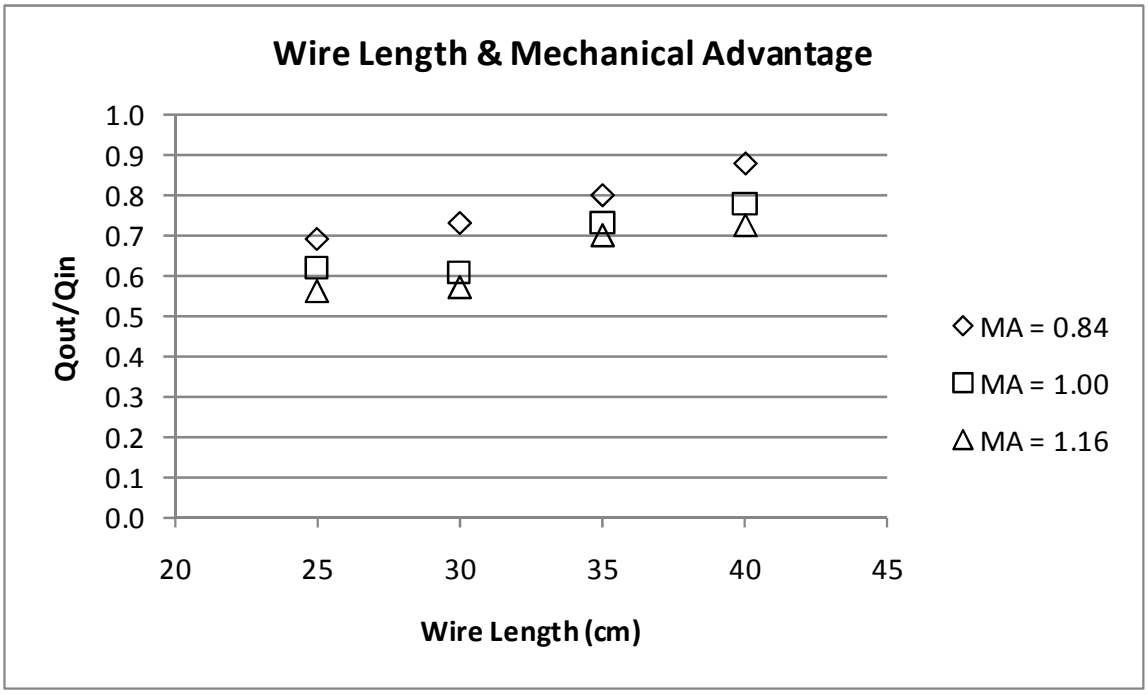

Figure 5.3 Fluid-only experimental results of output-to-input ratio for varying wire lengths and mechanical advantage using optimal flow durations.

Figure 5.4 compares the output-to-input ratios of the experimental results and simulation results when the mechanical advantage is 0.84, which yields higher performance than other mechanical advantages. As is evident from the plot, the simulation results are within 5% to 10% of the experimental results. This is satisfactory and should provide confidence for those using the model for fluid-only actuation in the future. Due to the physical limitations of the prototype, the performance of 45 cm and 50 cm actuators could not be explored.

Since the performance of the fluid-only experiments did not exceed an output-to-input ratio greater than one, electrical actuation assistance is required. After performing the fluid-only experiments, electrical actuation tests were then performed by varying flow duration for 40 cm actuators with a mechanical advantage of 0.84. All electrical actuation tests were performed with lead times in accordance with the maximum simulation results

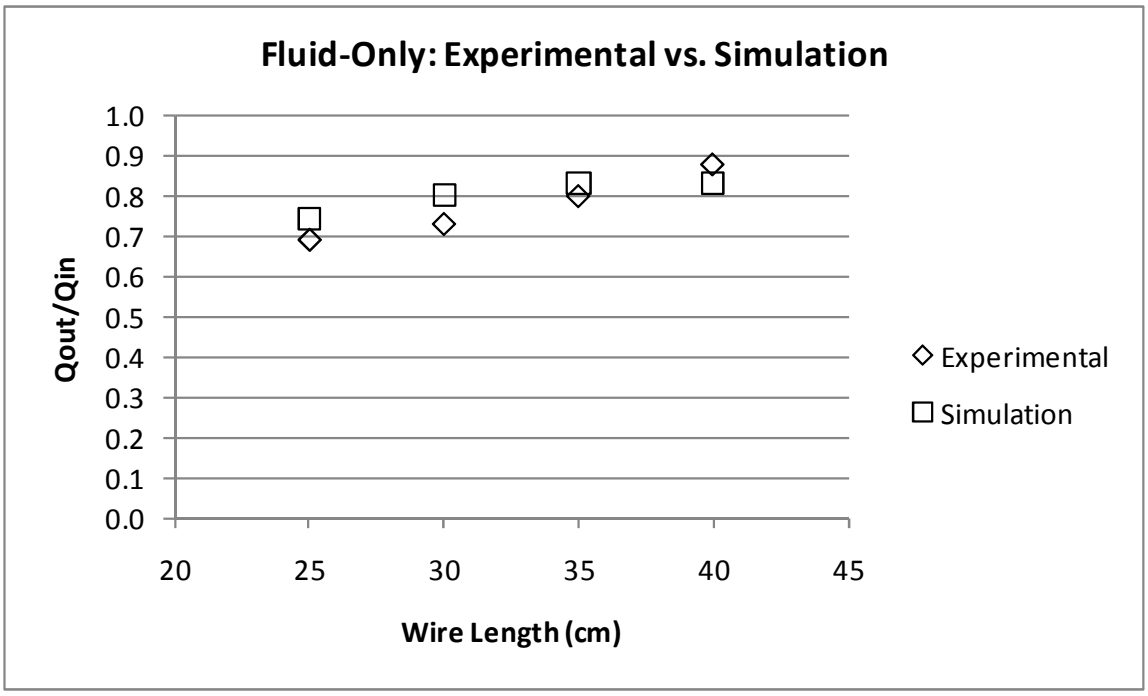

Figure 5.4 Comparison of experimental and simulation results of output-to-input ratio for optimal configurations of fluid-only actuation.

achieved for each flow duration in section 4.3.4 which suggests the best performance is reached with no lead time except when the flow duration is 1.5 seconds, at which point the optimal lead time is 0.5 seconds.

A comparison of the experimental and simulation output-to-input performance results is provided in Figure 5.5. It is evident that the model is able to predict the experimental performance with some accuracy for longer flow durations. Conversely, the model drastically underestimates the performance when the flow duration is 1.0 seconds. This could be a consequence of multiple complex interactions within the model. Further analysis of the water flow suggests that the hot water does reach the end of the actuator, but does not seem cause a significant phase transformation in the actual wire. This could be a result of inaccuracies in the thermal time constants of the fluid, wire, and tubing. These results provide insight to how necessary it is to combine fluid and electrical

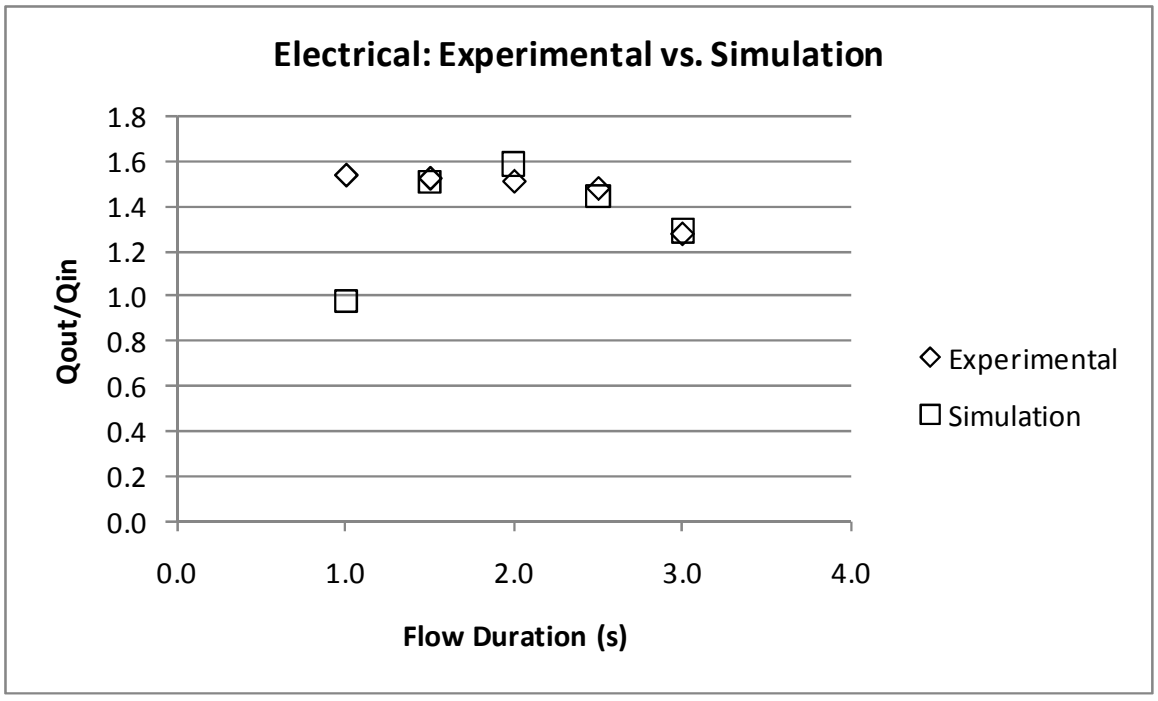

Figure 5.5 Comparison of experimental and simulation results of output-to-input ratio for optimal configurations of electrical actuation.

actuation in order to reach higher output performance.

The maximum output-to-input ratio reached experimentally with fluid and electrical actuation was 1.54 under the conditions provided. This performance meets the requirements necessary to provide fluid actuation to other subsystems while being able to still provide self-actuation. With this, the focus of the project in the future can begin to integrate the pump with other subsystems along with improving the efficiency and performance of the pump. This will be discussed in greater detail later in section 6.2.

5.3 Heat Addition and Power Requirements

Without continuous heat addition to the system, the performance of the pump degrades over time. Conversely, with heat input, the performance is expected to be sustained and even exceed that of the nonheated system. This is because the boiling point of the water will be higher due to the increased pressure within the accumulators as shown in Figure 3.9. The output-to-input ratio over time for fluid-only actuation with 40 cm actuators with and without heat addition is provided in Figure 5.6.

In the figure, it is readily noticeable that the performance begins to degrade significantly after roughly two minutes of pumping without additional heat. This can be remedied by inserting a heater coil into the hot water accumulator and insulating it. The results in the figure show that this is true and that the performance is significantly higher as expected. In this case, the output-to-input performance is sustained at almost 1.4 which is higher than predicted by simulation results provided in Figure 4.8 for higher boiling points of water. Due to the high output of the pump, the power required to sustain performance for fluid-only actuation is 323 Watts as obtained by using equation 3.7 and neglecting heat loss due to insulation of the hot accumulator. At this performance level,

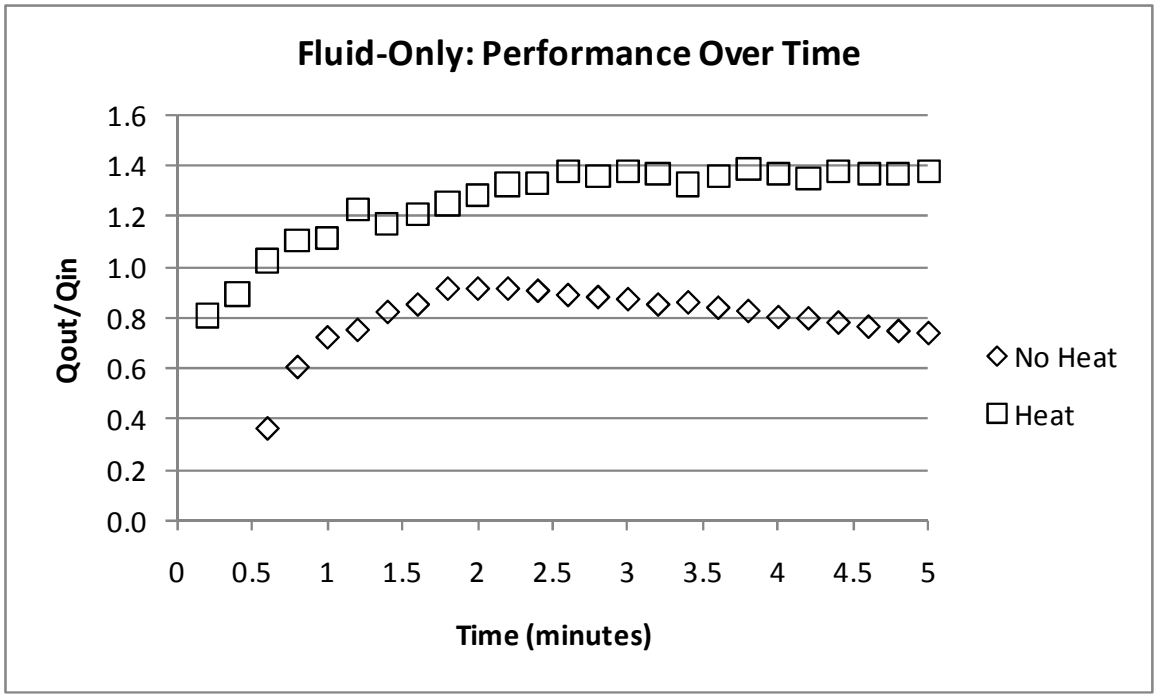

Figure 5.6 Performance over time with fluid-only actuation and 40 cm actuators with and without heat input to the hot accumulator water.

the pump is capable of pumping a net output of 24 mL/min.

Figure 5.7 is a plot that compares the piston position output from the potentiometer attached to the fulcrum of the lever on the pump for heated and nonheated hot water accumulator tests provided in Figure 5.6. Due to the increased boiling point of the water within the heated accumulator, the actuator strain is increased as is evident by the position in the figure. The nonheated accumulator test shows smaller peaks in position indicating less strain in the actuator. Although the maximum contraction that can occur for a 40 cm actuator is 16 mm (4% strain), the highest actual contraction observed was 11.5 mm (2.9% strain) with fluid-only actuation. This is due to the heat loss in the water before it reaches the actuators' end. Again, this can be mitigated by implementing electrical actuation to ensure full phase transformation along the entire SMA wire length.

Figure 5.8 is a plot showing the output-to-input performance over time with

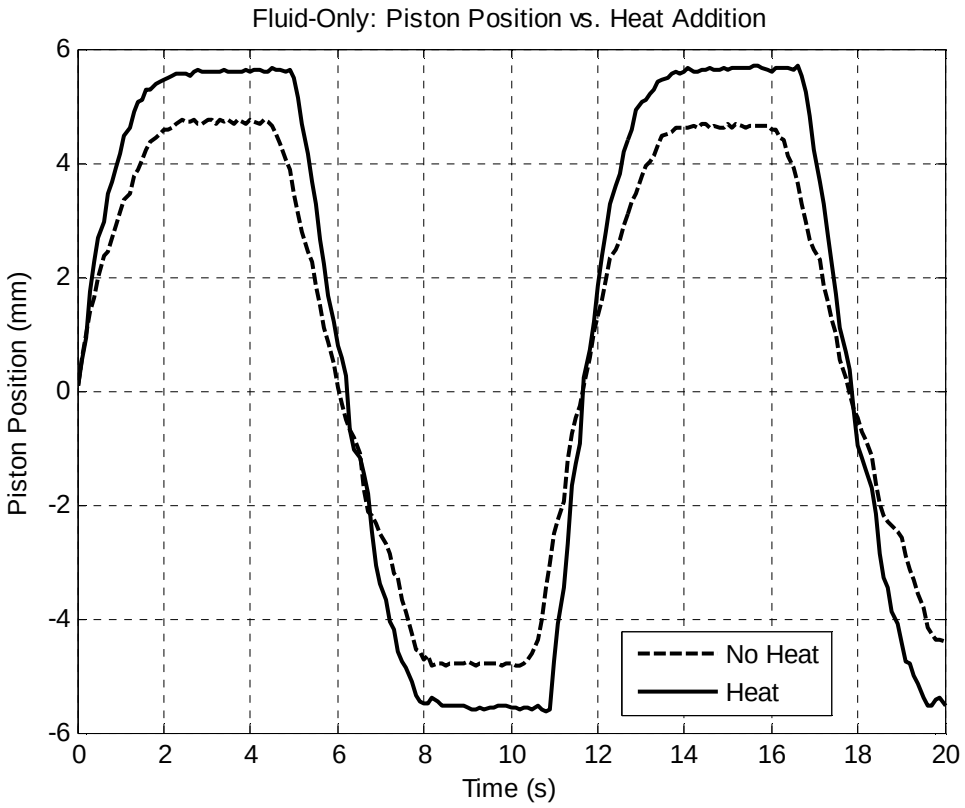

Figure 5.7 Comparison of the piston position over time for test with and without heat addition to the hot water accumulator using fluid-only actuation.

electrical actuation. Similarly with fluid-only actuation, the performance is significantly greater with heat added and the performance is also sustained. The maximum performance reached with 40 cm actuators and electrical actuation is roughly 2.1. The flow duration is 1.5 seconds without any electrical lead time.

The total power requirement to sustain this performance with electrical actuation is 520 Watts and neglecting heat loss from the hot accumulator. Nearly 93% of this power goes into the maintaining the temperature inside the hot accumulator while only 7% is needed for electrical actuation. This power required is significantly higher than that of the fluid-only configuration primarily because of the increased fluid output of the pump. With this configuration, the pump is capable of pumping a net output up to 66 mL/min.

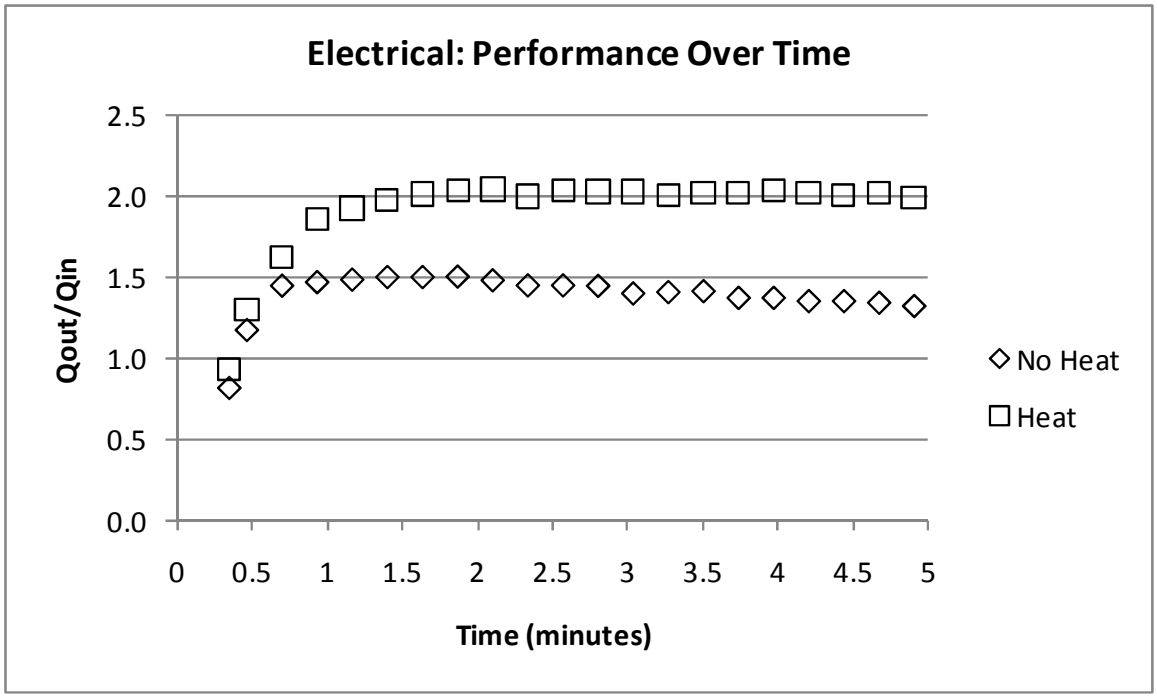

Figure 5.8 Performance over time with electrical actuation and 40 cm actuators with and without heat input to the hot accumulator water.

5.4 Pump Efficiency and Power Density

While the power required for the configuration with electrical actuation is significantly higher than that with fluid-only, the efficiency is also higher. The net power efficiency of the electrical actuation configuration is 0.0032% while the efficiency of the fluid-only configuration is 0.0019%. These values were obtained using equation 3.8 and do not include the small amount of power required (approximately 1 Watt) to activate the solenoid valves. As is evident, these efficiencies are not high and require improvement in future designs. Ways of improving these efficiencies would be to improve the expected output performance by using alternative pump designs, some of which were discussed in section 3.1. The peristaltic concept particularly suggests increased output.

The power density of the fluid-only pump is 0.0016 W/kg (0.0025 W/L) while the

power density of the electrical pump configuration is 0.0043 W/kg (0.0068 W/L). These are significantly small as well, but can be increased by increasing the output of the pump and decreasing the pump mass and volume. Components that make up the majority of the mass and volume are the frame and the pumping chambers. Using alternate materials and smaller dimensions would decrease the mass and volume significantly and increase the power density by an order of magnitude. Additionally, although the efficiency of the pump is low, making the use of high density energy storage can improve overall power density. One author uses high energy dense fuels to heat the water used to actuate SMA actuators [10]. Table 5.1 summarizes the values required to calculate the efficiency and power density of the fluid-only and electrical actuation configurations.

Figure 5.9 is a plot that compares the wet SMA pump to other types of common pumps including the human heart as presented in Figure 1.3. It is desired to reach levels similar to the human heart, but this has not yet been accomplished. There may be other designs not yet developed that could improve both the efficiency of the power density.

Table 5.1 Summary of values used for calculating the power efficiency and density of the fluid-only and electrical actuation configurations.

Symbol	Parameter	Fluid-Only	Electrical	Units
P_{accum}	Accumulator Pressure	15000	15000	Pa
Q_{out}	Pump Output	1.4	2.1	mL/s
Q_{in}	Pump Input	1	1	mL/s
P_{in}	Power Required	323	520	W
m_P	Pump Mass	3.81	3.81	kg
V_P	Pump Volume	2400	2400	mL
η_p	Efficiency	0.0019%	0.0032%	-
p_m	Mass Power Density	0.0016	0.0043	W/kg
p_V	Volume Power Density	0.0025	0.0068	W/L

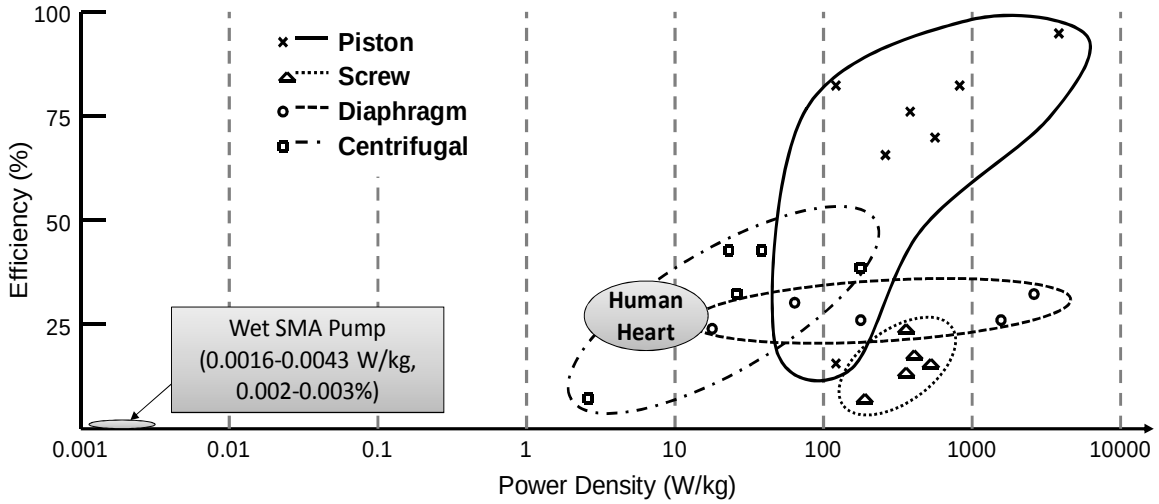

Figure 5.9 Comparison of efficiencies and mass power densities of common pumps to the wet SMA pump. See Appendix B for more information.

5.5 Conclusions

It has been shown by simulation and experimentation that the SMA pump is capable of providing a sufficient amount of fluid to actuate external SMA systems. This is evident by the output-to-input ratios of the pump being 1.4 for fluid-only actuation and 2.1 with electrical assistance. It has been demonstrated that the pump can sustain performance over long periods of time with continuous heat addition to the hot water accumulator. The fluid-only pump configuration requires 323 Watts to sustain performance and is 0.0019% efficient. The electrical configuration requires 520 Watts and is 0.0032% efficient. The power densities of the fluid-only and electrical pump configuration are 0.0016 W/kg (0.0025 W/L) and 0.0043 W/kg (0.0068 W/L), respectively. By modifying the current chamber design and using lighter materials, both the efficiency and power density can be improved. The pump is capable of pumping a net output of 66 mL/min.

CHAPTER 6

CONCLUSIONS

6.1 Summary

The goal of this thesis was to create a biologically inspired wet shape memory alloy actuated pump that could provide thermal energy via fluidic convection to external wet SMA subsystems. Furthermore, the pump was to draw from its own thermofluidic output to assist in actuating its own internal SMA actuators. A thorough analysis of the previous wet SMA robotic heart has been conducted by searching for opportunities for improvement. Methods of improving output as well as decreasing pump input were explored by modifying the pumping chambers, actuation timing, and continuously adding heat to the system.

In an effort to accurately represent the design changes and future testing results, modifications to the previous dynamic model were made that include temperature dependent properties, a more comprehension phase hysteresis curve, and the capability of being able to model complex timing with electrical actuation occurring. Modeling results were provided as a baseline indicator of what was to be expected during actual implementation and testing. The effects of changing various parameters were explored to determine optimal configurations in order to eliminate unnecessary testing. Key parameters found include using small mechanical advantages, actuator lengths of 40 cm,

and flow durations long enough to cause optimal contraction. Water temperature was found to play a large role in output-to-input ratio. Electrical actuation modeling results indicated an output-to-input ratio greater than 1.0, suggesting the wet SMA pump becoming a viable robotic heart device.

Implemented design changes and testing confirmed the modeling results. With fluid-only actuation, the output-to-input ratio did not exceed 1.0 except when the hot water was heated within the accumulator. With heating, the performance peaked at nearly 1.4. The pump reached an output-to-input performance of nearly 1.6 with electrical actuation and when continuous heat was added, the performance reached almost 2.1. These output-to-input ratios indicate the wet SMA pump is able to pump more fluid than it consumes for actuation. That makes this pump the first heart-like self-sustaining SMA pump ever built. It is also the first SMA pump capable of distributing thermal fluids to external wet SMA subsystems on a macroscale by pumping a net output of 66 mL/min as opposed to micro SMA pumps that can only pump on an order of 1 mL/min or less.

Although the pump's output-to-input ratio far exceeds 1.0, the power efficiency and power density of the pump are far below what was desired. It was desired to reach levels similar to the human heart, but the amount of power required to keep the hot water continuously heated at boiling point limited the efficiency considerably. As mentioned previously in section 1.1, the maximum possible efficiency of the actuators themselves is on the order of 3% and 0.2% when taking heat loss into account. The reasons for this large difference in efficiency is that in the SMA pump, the hot water travels through much more tubing and is held in a reservoir for a period of time before it is pumped through more tubing, into the pumping chambers, and finally back into the hot water

accumulator.

Options for improving efficiency and power density include insulating the accumulators, pumping chambers, reservoirs, actuators, and all of the tubing. This will minimize heat loss as explained in section 3.5. Other methods of improving efficiency include minimizing pump mass, optimizing pumping chamber design, and reducing the amount of heat necessary to keep the hot water at an elevated temperature by using insulation, and finding an alternate fluid that can operate at higher temperatures with a low viscosity.

6.2 Recommendations for Future Work

Although the pump was able to exceed an output-to-input ratio greater than unity, there are still some aspects of the pump that need to be further developed in order to fully realize the entire pump system and integrate it with other subsystems as a viable method of actuating separate SMA mechanisms. The opportunities for future work are integration with other subsystems, increasing the pump mobility, and increasing the pump's output performance. First, integration with other subsystems requires that the pump be somewhat transportable and must have enough outlets from the accumulators to supply hot and cold fluid to other mechanisms. This also requires a more complex timing and feedback system in order to adequately control and monitor other subsystems.

Concerning mobility, the robotic pump currently relies on computer control via LabVIEW to keep the timing of the separate actuators. This type of software control can be costly and requires an entire computer system to be attached to the robotic pump. There are a couple of ways to remove this necessity. One method would be to implement mechanical switching of the hot and cold fluid to the actuators based on lever or actuator

position. This would eliminate the need for extra electrical power to activate the solenoid valves. Another would be to implement the timing control via a microcontroller with timing capability. It is also necessary to remove the need to rely on external heating and pressure regulation sources inside the accumulators.

With regards to improving output-to-input ratio and pump efficiency, there are still many things that can be done to improve the overall output performance of the pump. One approach would be to optimize the pumping chamber diameter and the diaphragm thickness. Simulations suggest that by increasing the pumping chamber diameter within a given range while maintaining a relatively low fluidic capacity due to bulging that the pump output should increase significantly. The downside to this is that machining of the chambers can be expensive and would require redesigning the diaphragms accordingly.

Another way to potentially increase the performance of the pump would be to research more alternate fluids that would have high boiling points and thermal conductivities while at the same time having low enough viscosities that would allow for low accumulator pressures. As mentioned in section 3.3, glycerol and ethylene glycol were too viscous to be used efficiently.

The final recommendation for increased performance of the SMA robotic pump would be to implement the peristaltic pump concept outlined in section 3.1.2 or the dual bellows pump outlined in section 3.1.3. Both of these concepts have shown a higher potential output per unit length of SMA wire, but the implementation of these pumps may prove to be quite challenging. An implementation of a SMA peristaltic pump has been developed [23-25] and could be used as a starting point for future SMA pump development.

APPENDIX A

PUMP EFFICIENCY DATA

Table A.1 Table of power densities and efficiencies for various types of pumps.

Pump Type	Manufacturer	Model	Power Density (W/kg)	Efficiency
Piston	Cat Pumps	280 [36]	160	81%
	Rexroth	A2FO-5 [37]	5796	95%
	Cole-Parmer	EW-07143-73 [38]	105	6%
	Annovi Reverberi	RMV2.5G20 [39]	940	85%
	Annovi Reverberi	SJV 3400 [40]	545	81%
	Sauer Danfoss	Series 45-L25C [41]	750	68%
	Ingersoll Rand	650939-X4D-B [42]	286	60%
Screw	IMO Pump	Series 3E-87P [43]	326	2%
	IMO Pump	Series 6T-250 [44]	600	17%
	Leistritz	L3 [45]	550	27%
	Warren Pumps	211 Series [46]	775	15%
Diaphragm	Graco	Huskey 205 [47]	1304	23%
	Wilden Pumps	P100 [48]	76	38%
	Flojet	02100-12C [49]	12	25%
	Grundfos	DME Series [50]	216	27%
	Hydra-Cell	F/G-20-X [51]	2300	31%
Centrifugal	Little Giant	1-A [52]	2.5	3%
	Dayton	4HFA7 [53]	11.5	16%
	Dayton	2YEV3 [54]	300	38%
	Dayton	2ZWZ1 [55]	37	41%
	Cole-Parmer	EW-07085-00 [38]	43	46%
	IPT	2SSBP 3000 [56]	20.7	32%

APPENDIX B

MATLAB CODE FOR ROBOTIC PUMP SIMULATIONS

B.1 Code for "pumpsim.m"

```
% This script runs "temp2rm.m" which solves the thermal model and
% martensite fraction-temperature profile. It then calls an ODE solver
% to solve "pumpsys.m" which is the complete robotic pump system.


clear all;
close all;
clc;

global Rm1 Rm2 t n t_on t_off t_es t_elec L Ma

L = .40;        % Actuator length, m
Ma = 0.84;      % Mechanical Advantage

% Fluid Timiing
t_on = 2.0;     % Fluid Flow ON
t_off = 1.0;    % Fluid Flow OFF

% Electricity Timing
% t_on = 2.0;     % Fluid Flow ON
% t_es = 2.0;     % Electricity Start Time (t_es >= t_on - t_elec)
% t_elec = 1;     % Electricity Time ON (t_elec <= t_off)
% t_off = t_es+t_elec+1-t_on;

cycles = 3;     % Number of Cycles to Model

% Solve temperature and martensite fraction profiles
temp2rm;
% temp2rm_elec;

% Pump initial conditions
F1o = 20*ones(n,1);
F2o = 20*ones(n,1);
Pa0 = 0;
Pb0 = 0;
Vm0 = 0;
Xm0 = 0;

% Solve pump system eqns
y0 = [F1o; F2o; Pa0; Pb0; Vm0; Xm0; 0; 0; 0; 0];
tspan = t;
options = odeset('RelTol',1e-3,'AbsTol',1e-6);
[time,y] = ode23tb(@pumpsys,tspan,y0,options);
```

```
% Sort y0 results
F1 = y(:,1:n);
F2 = y(:,n+1:2*n);
Pa = y(:,2*n+1);
Pb = y(:,2*n+2);
Vm = y(:,2*n+3);
Xm = y(:,2*n+4);
V1out = y(:,2*n+5);
V2out = y(:,2*n+6);
V1in = y(:,2*n+7);
V2in = y(:,2*n+8);

% Flow output & feasibility
%Qout = (max(V1out) + max(V2out))/max(time);    % Cylindrical Pumping
Qout = .495*(max(V1out) + max(V2out))/max(time);    %.495 Accounts for
Conical Pumping
Qin = 2*t_on/(t_on+t_off)*Q;
eff = Qout/Qin

% % Plot Results
figure(1);
plot(time,Rm1,time,Rm2);
ylim([0 1]);
ylabel('Martensite Fractions');
xlabel('Time (sec)');
%legend('Hot','Cold');

figure(2);
plot(time,F1(:,1),'-k',time,F2(:,1),'-.k');
ylabel('Actuator Forces (N)');
xlabel('Time (sec)');
legend('Hot','Cold');

figure(3);
plot(time,Pa,'-k',time,Pb,'-.k');
ylabel('Chamber Pressures (Pa)');
xlabel('Time (sec)');
legend('Hot','Cold');

figure(4);
subplot(2,1,1);
plot(time,Xm,'-k');
ylabel('Piston Position (m)');
xlabel('Time (sec)');

subplot(2,1,2);
plot(time,Vm,'k');
ylabel('Piston Velocity (m/s)');
xlabel('Time (sec)');

figure(5);
subplot(2,1,1);
plot(time,V1out,'-k',time,V2out,'-.k')
ylabel('V_o_u_t');
xlabel('Time (sec)');
legend('Hot','Cold');

subplot(2,1,2);
plot(time,V1in,'-k',time,V2in,'-.k');
ylabel('V_i_n');
xlabel('Time (sec)');
legend('Hot','Cold');

figure(6);
```

```
axis([0 1 0 1]);
text(.3,.7,strcat('Qout =',num2str(Qout)));
text(.3,.5,strcat('Qin =',num2str(Qin)));
text(.3,.3,strcat('Qout/Qin =',num2str(eff)));
```

B.2 Code for "temp2rm.m"

```
% This program is run by "pumpsim.m" to calculate the temperature and
% martensite profiles for two opposing SMA actuators using water-only
% actuation.

% Declare global variables
global Rm1 Rm1dot Rm2 Rm2dot t dt m n Dw dx Sp Rv R L Ea Em Et Ed eym
edm M Ma Ac C K t_on t_off

% Wire properties
Dw = .02*.0254; % Wire diameter, m
pw = 6450;      % SMA density, kg/m^3
cpw = 837;      % SMA specific heat, J/(kg*K) 837
Twi = 24;       % Initial wire temperature, C
Abar = 78;      % Avg Forward transformation temp, C
sa = 9;         % StDev Forward transformation temp, C
Mbar = 55;      % Avg Reverse transformation temp, C
sm = 6;         % StDev Reverse transformation temp, C
Ea = 37494e6;   % Austenite modulus of elasticity, Pa
Em = 12214e6;   % Twinned martensite modulus, Pa
Et = 638.6e6;   % Partially twinned martensite modulus, Pa
Ed = 7800e6;    % Detwinned martensite modulus, Pa
eym = .00399;   % Maximum strain of twinned martensite
edm = .0417;    % Minimum strain of detwinned martensite
R = 10;         % Damping coefficient, N/s

% Tube properties
Df = .0625*.0254;   % Tube inner diameter, m
Dt = .125*.0254;    % Tube outer diameter, m
pt = 1290;          % Tube density, kg/m^3
cpt = 1460;         % Tube specific heat, J/(kg*K)
K = 50;

% Fluid properties
cpf = 4200;         % Fluid specific heat, J/(kg*K)
Tfh = 88;           % Hot fluid temperature, C
Tfc = 24;           % Cold fluid temperature, C
visc = 5.468e-4;    % Dynamic Fluid viscosity, Pa*s
pf = 998;           % Fluid density, kg/m^3
Pr = 3.55;          % Fluid Prandtl number
kf = .643;          % Fluid thermal conductivity, W/(m*K)
% see kf(T) and cpf(T) below

% Air properties
Ta = 24;            % Ambient temperature, C
ka = 28.1e-3;       % Air thermal conductivity, W/(m*K)

% System properties
Nua = 30;                   % Ambient Nusselt number, Nu_a
M = .3;                     % Suspended mass, kg
Ac = 15.5e-4;               % Pumping chamber cross-sectional area, m^2
Rv = 3e9;                   % Pumping Chamber Fluid Resistance, Pa*s/m^3
C = 5e-10;                  % Pumping Chamber Capacitance (pg 53 - 54)
Rf = 1.5e10;                % Actuator fluidic resistance, Pa*s/m^3
Sp = 15000;                 % Accumulator pressure, Pa
```

```
Q = Sp/Rf;                  % Flow rate, m^3/s
uf = Q/(pi/4*(Df^2-Dw^2)); % Average fluid velocity, m/s
Re = pf*uf*(Df-Dw)/visc;   % Reynolds number
ts = t_on+t_off;           % Hot/Cold duration, sec

% n = Number of Actuator Nodes
% dx = Distance the boundary moves each iteration of outer loop
% dt = Time that passes during each iteration
% m = Number of Time Steps
n = 20;
dx = L/(n-1);
dt = dx/uf;
m = ceil(cycles*2*ts/dt);

% Set initial profiles
Tw_l1 = Twi*ones(1,n);  % Wire
Tf_l1 = Twi*ones(1,n);  % Fluid
Tt_l1 = Twi*ones(1,n);  % Tube
Tw_l2 = Twi*ones(1,n);  % Wire
Tf_l2 = Twi*ones(1,n);  % Fluid
Tt_l2 = Twi*ones(1,n);  % Tube

Rm1 = zeros(m,n);
Rm2 = zeros(m,n);
Rm1dot = zeros(m,n);
Rm2dot = zeros(m,n);

for j = 1:m

    % Track time and boundary position
    t(j) = dt*(j-1);

    for i = 1:n
        l(i) = dx*(i-1);

        % Calculate Nusselt numbers and thermal time constants
        Nuo = 4;    % Nu_f
        Nui(i) = 16.64*exp(-16.44*l(i))+8.52; % Nu_w (Experimental)

        % Calculate coefficients for actuator #1
        T = Tf_l1(i);
        kf = -7.42e-6*T^2+1.86e-3*T+.569; % kf(T)
        cpf = (1.92e-9*T^4-4.89e-7*T^3+5.34e-5*T^2-2.29e-...
            3*T+4.21)*1000; %cpf(T)
        c1 = 4*Nui(i)*kf/(cpw*pw*Dw*(Df-Dw)); % 1/tau_w,f
        c2 = 4*Nui(i)*kf*Dw/(cpf*pf*(Df-Dw)*(Df^2-Dw^2)); % 1/tau_f,w
        c3 = 4*Nuo*kf*Df/(pf*cpf*(Df-Dw)*(Df^2-Dw^2)); % 1/tau_f,t
        c4 = 4*Nuo*kf*Df/(pt*cpt*(Df-Dw)*(Dt^2-Df^2)); % 1/tau_t,f
        c5 = 4*Nua*ka/(pt*cpt*(Dt^2-Df^2)); % 1/tau_t,a

        % Calculate temperture changes for actuator #1
        delTw1(j,i) = (c1*(Tf_l1(i)-Tw_l1(i)))*dt;
        delTf1(i) = (c2*(Tw_l1(i)-Tf_l1(i))+c3*(Tt_l1(i)-Tf_l1(i)))*dt;
        delTt1(i) = (c4*(Tf_l1(i)-Tt_l1(i))+c5*(Ta-Tt_l1(i)))*dt;

        % Calculate coefficients for actuator #2
        T = Tf_l2(i);
        kf = -7.42e-6*T^2+1.86e-3*T+.569; % kf(T)
        cpf = (1.92e-9*T^4-4.89e-7*T^3+5.34e-5*T^2-2.29e-...
            3*T+4.21)*1000; %cpf(T)
        c1 = 4*Nui(i)*kf/(cpw*pw*Dw*(Df-Dw)); % 1/tau_w,f
        c2 = 4*Nui(i)*kf*Dw/(cpf*pf*(Df-Dw)*(Df^2-Dw^2)); % 1/tau_f,w
        c3 = 4*Nuo*kf*Df/(pf*cpf*(Df-Dw)*(Df^2-Dw^2)); % 1/tau_f,t
        c4 = 4*Nuo*kf*Df/(pt*cpt*(Df-Dw)*(Dt^2-Df^2)); % 1/tau_t,f
```

```
c5 = 4*Nua*ka/(pt*cpt*(Dt^2-Df^2)); % 1/tau_t,a

% Calculate temperture changes for actuator #2
delTw2(j,i) = (c1*(Tf_l2(i)-Tw_l2(i)))*dt;
delTf2(i) = (c2*(Tw_l2(i)-Tf_l2(i))+c3*(Tt_l2(i)-Tf_l2(i)))*dt;
delTt2(i) = (c4*(Tf_l2(i)-Tt_l2(i))+c5*(Ta-Tt_l2(i)))*dt;

% Add temp change to old temp
Tw_l1(i) = Tw_l1(i) + delTw1(j,i);
Tf_l1(i) = Tf_l1(i) + delTf1(i);
Tt_l1(i) = Tt_l1(i) + delTt1(i);
Tw1(j,i) = Tw_l1(i);
Tw_l2(i) = Tw_l2(i) + delTw2(j,i);
Tf_l2(i) = Tf_l2(i) + delTf2(i);
Tt_l2(i) = Tt_l2(i) + delTt2(i);
Tw2(j,i) = Tw_l2(i);

% Calculate martensite fraction profile
if j == 1
    Rm1(j,i) = 1;
    Rm2(j,i) = 1;
else

    % Determine heating or cooling curve from sign of
    % temperature rate.
    hf1 = .5*(1+erf((Tw1(j,i)-Abar)/(sa*sqrt(2)))); % Fwd
    hr1 = .5*(1+erf((Tw1(j,i)-Mbar)/(sm*sqrt(2)))); % Rev
    hf2 = .5*(1+erf((Tw2(j,i)-Abar)/(sa*sqrt(2)))); % Fwd
    hr2 = .5*(1+erf((Tw2(j,i)-Mbar)/(sm*sqrt(2)))); % Rev

    % Calculate Rm for the actuators
    if delTw1(j,i) == 0
        Rm1(j,i) = Rm1(j-1,i);
    elseif delTw1(j,i) > 0
        g = exp(-(Tw1(j,i)-Abar)^2/(2*sa^2))/sa/sqrt(2*pi);
        Rm1(j,i) = Rm1(j-1,i)+(hr1+Rm1(j-1,i)-1)/(hf1-...
          hr1)*g*delTw1(j,i);
    elseif delTw1(j,i) < 0
        g = exp(-(Tw1(j,i)-Mbar)^2/(2*sm^2))/sm/sqrt(2*pi);
        Rm1(j,i) = Rm1(j-1,i)+(hf1+Rm1(j-1,i)-1)/(hr1-...
          hf1)*g*delTw1(j,i);
    end

    if delTw2(j,i) == 0
        Rm2(j,i) = Rm2(j-1,i);
    elseif delTw2(j,i) > 0
        g = exp(-(Tw2(j,i)-Abar)^2/(2*sa^2))/sa/sqrt(2*pi);
        Rm2(j,i) = Rm2(j-1,i)+(hr2+Rm2(j-1,i)-1)/(hf2-...
          hr2)*g*delTw2(j,i);
    elseif delTw2(j,i) < 0
        g = exp(-(Tw2(j,i)-Mbar)^2/(2*sm^2))/sm/sqrt(2*pi);
        Rm2(j,i) = Rm2(j-1,i)*(1+(hf2+Rm2(j-1,i)-1)/(hr2-...
          hf2)*g*delTw2(j,i));
    end

    if isnan(Rm1(j,i)) || abs(Rm1(j,i)) == Inf
        Rm1(j,i) = Rm1(j-1,i);
    elseif Rm1(j,i) < 0
        Rm1(j,i) = 0;
    elseif Rm1(j,i) > 1
        Rm1(j,i) = 1;
    end

    if isnan(Rm2(j,i)) || abs(Rm2(j,i)) == Inf
```

```
                Rm2(j,i) = Rm2(j-1,i);
            elseif Rm2(j,i) < 0
                Rm2(j,i) = 0;
            elseif Rm2(j,i) > 1
                Rm2(j,i) = 1;
            end

        end

    end

    % Fluid temperature control/switching
    count = floor(t(j)/ts);
    count2 = rem(count,2);

    % Fluid inlet temperature after passing through tubing
    r = .8163;
    tau1 = .11;
    tau2 = .35;

    if ~count2
        Tfe1 = (Tfh-Tfc)*(r*(1-exp(-1/tau1*(t(j)-ts*count)))+(1-r)*...
            (1-exp(-1/tau2*(t(j)-ts*count))))+Tfc;
        Tfe2 = (Tfc-Tfh)*(r*(1-exp(-1/tau1*(t(j)-ts*count)))+(1-r)*...
            (1-exp(-1/tau2*(t(j)-ts*count))))+Tfh;
    else
        Tfe1 = (Tfc-Tfh)*(r*(1-exp(-1/tau1*(t(j)-ts*count)))+(1-r)*...
            (1-exp(-1/tau2*(t(j)-ts*count))))+Tfh;
        Tfe2 = (Tfh-Tfc)*(r*(1-exp(-1/tau1*(t(j)-ts*count)))+(1-r)*...
            (1-exp(-1/tau2*(t(j)-ts*count))))+Tfc;
    end

    if t(j) < 1
        Tfe2 = Ta;
    end

    % Advance Fluid for t_on seconds
    if rem(t(j),ts) <= t_on
        Tf_l1 = [Tfe1 Tf_l1(1:n-1)];
        Tf_l2 = [Tfe2 Tf_l2(1:n-1)];
    end

end

for i = 1:n
    Rm1dot(:,i) = deriv(Rm1(:,i),t,1);
    Rm2dot(:,i) = deriv(Rm2(:,i),t,1);
end
```

B.3 Code for “temp2rm_elec.m”

```
% This program is run by "pumpsim.m" to calculate the temperature and
% martensite profiles for two opposing SMA actuators using water and
% electrical actuation.

% Declare global variables
global Rm1 Rm1dot Rm2 Rm2dot t m n Dw dx Sp Rv R L Ea Em Et Ed eym edm
M Ma Ac C K t_on t_off t_es t_elec

% Wire properties
Dw = .02*.0254; % Wire diameter, m
```

```
pw = 6450;      % SMA density, kg/m^3
cpw = 837;      % SMA specific heat, J/(kg*K)
Twi = 24;       % Initial wire temperature, C
Abar = 78;      % Avg Forward transformation temp, C
sa = 9;         % StDev Forward transformation temp, C
Mbar = 55;      % Avg Reverse transformation temp, C
sm = 6;         % StDev Reverse transformation temp, C
Ea = 37494e6;   % Austenite modulus of elasticity, Pa
Em = 12214e6;   % Twinned martensite modulus, Pa
Et = 638.6e6;   % Partially twinned martensite modulus, Pa
Ed = 7800e6;    % Detwinned martensite modulus, Pa
eym = .00399;   % Maximum strain of twinned martensite
edm = .0417;    % Minimum strain of detwinned martensite
R = 10;         % Damping coefficient, N/s
Ve = 7.75;      % Power Supply Voltage (7.75)
Re = 4.3;       % Electrical Resistance, Ohms/m (4.3)
Ie = Ve/Re/L;   % Electrical Current, A (4.5)

% Tube properties
Df = .0625*.0254;   % Tube inner diameter, m
Dt = .125*.0254;    % Tube outer diameter, m
pt = 1290;          % Tube density, kg/m^3
cpt = 1460;         % Tube specific heat, J/(kg*K)
K = 50;

% Fluid properties
cpf = 4200;         % Fluid specific heat, J/(kg*K)
Tfh = 88;           % Hot fluid temperature, C
Tfc = 24;           % Cold fluid temperature, C
visc = 5.468e-4;    % Dynamic Fluid viscosity, Pa*s
pf = 998;           % Fluid density, kg/m^3
Pr = 3.55;          % Fluid Prandtl number
kf = .643;          % Fluid thermal conductivity, W/(m*K)
% see kf(T) and cpf(T) below

% Air properties
Ta = 24;            % Ambient temperature, C
ka = 28.1e-3;       % Air thermal conductivity, W/(m*K)

% System properties
Nua = 30;                   % Ambient Nusselt number, Nu_a
M = .3;                     % Suspended mass, kg
Ac = 15.5e-4;               % Pumping chamber cross-sectional area, m^2
Rv = 3e9;                   % Pumping Chamber Fluid Resistance, Pa*s/m^3
C = 5e-10;                  % Pumping Chamber Capacitance (pg 53 - 54)
Rf = 1.5e10;                % Actuator fluidic resistance, Pa*s/m^3
Sp = 15000;                 % Accumulator pressure, Pa
Q = Sp/Rf;                  % Flow rate, m^3/s
uf = Q/(pi/4*(Df^2-Dw^2)); % Average fluid velocity, m/s
ts = t_on+t_off;            % Hot/Cold duration, sec

% n = Number of Actuator Nodes
% dx = Distance the boundary moves each iteration of outer loop
% dt = Time that passes during each iteration
% m = Number of Time Steps
n = 20;
dx = L/(n-1);
dt = dx/uf;
m = ceil(cycles*2*ts/dt);

% Set initial profiles
Tw_l1 = Twi*ones(1,n);  % Wire
Tf_l1 = Twi*ones(1,n);  % Fluid
Tt_l1 = Twi*ones(1,n);  % Tube
```

```
Tw_l2 = Twi*ones(1,n);  % Wire
Tf_l2 = Twi*ones(1,n);  % Fluid
Tt_l2 = Twi*ones(1,n);  % Tube

Rm1 = zeros(m,n);
Rm2 = zeros(m,n);
Rm1dot = zeros(m,n);
Rm2dot = zeros(m,n);

for j = 1:m

    % Track time and boundary position
    t(j) = dt*(j-1);    % Time
    cyc = rem(t(j),ts); % Time in Current Cycle

    % Fluid temperature control/switching
    count = floor(t(j)/ts);
    count2 = rem(count,2);

    for i = 1:n
        l = dx*(i-1);

        % Calculate Nusselt numbers and thermal time constants
        Nuo = 4; % Nu_f
        if cyc > t_on
            Nui = 8.83;
        else
            Nui = 16.64*exp(-16.44*l)+8.52; % Nu_w (Experimental)
        end

        % Calculate coefficients for actuator #1
        T = Tf_l1(i);
        kf = -7.42e-6*T^2+1.86e-3*T+.569; % kf(T)
        cpf = (1.92e-9*T^4-4.89e-7*T^3+5.34e-5*T^2-2.29e-...
            3*T+4.21)*1000; %cpf(T)
        c1 = 4*Nui*kf/(cpw*pw*Dw*(Df-Dw)); % 1/tau_w,f
        c2 = 4*Nui*kf*Dw/(cpf*pf*(Df-Dw)*(Df^2-Dw^2)); % 1/tau_f,w
        c3 = 4*Nuo*kf*Df/(pf*cpf*(Df-Dw)*(Df^2-Dw^2)); % 1/tau_f,t
        c4 = 4*Nuo*kf*Df/(pt*cpt*(Df-Dw)*(Dt^2-Df^2)); % 1/tau_t,f
        c5 = 4*Nua*ka/(pt*cpt*(Dt^2-Df^2)); % 1/tau_t,a

        % Calculate temperture changes for actuator #1
        delTw1 = c1*(Tf_l1(i)-Tw_l1(i))*dt;
        if (cyc > t_es) && (cyc < t_es+t_elec) && ~count2
            delTw1 = delTw1+Ie^2*Re/(pi/4*Dw^2*pw*cpw)*dt; % Electrical
        end
        delTf1 = (c2*(Tw_l1(i)-Tf_l1(i))+c3*(Tt_l1(i)-Tf_l1(i)))*dt;
        delTt1 = (c4*(Tf_l1(i)-Tt_l1(i))+c5*(Ta-Tt_l1(i)))*dt;

        % Calculate coefficients for actuator #2
        T = Tf_l2(i);
        kf = -7.42e-6*T^2+1.86e-3*T+.569; % kf(T)
        cpf = (1.92e-9*T^4-4.89e-7*T^3+5.34e-5*T^2-2.29e-...
            3*T+4.21)*1000; %cpf(T)
        c1 = 4*Nui*kf/(cpw*pw*Dw*(Df-Dw)); % 1/tau_w,f
        c2 = 4*Nui*kf*Dw/(cpf*pf*(Df-Dw)*(Df^2-Dw^2)); % 1/tau_f,w
        c3 = 4*Nuo*kf*Df/(pf*cpf*(Df-Dw)*(Df^2-Dw^2)); % 1/tau_f,t
        c4 = 4*Nuo*kf*Df/(pt*cpt*(Df-Dw)*(Dt^2-Df^2)); % 1/tau_t,f
        c5 = 4*Nua*ka/(pt*cpt*(Dt^2-Df^2)); % 1/tau_t,a

        % Calculate temperture changes for actuator #2
        delTw2 = c1*(Tf_l2(i)-Tw_l2(i))*dt;
        if (cyc > t_es) && (cyc < t_es+t_elec) && count2
            delTw2 = delTw2+Ie^2*Re/(pi/4*Dw^2*pw*cpw)*dt; % Electrical
```

```
end
delTf2 = (c2*(Tw_l2(i)-Tf_l2(i))+c3*(Tt_l2(i)-Tf_l2(i)))*dt;
delTt2 = (c4*(Tf_l2(i)-Tt_l2(i))+c5*(Ta-Tt_l2(i)))*dt;

% Add temp change to old temp
Tw_l1(i) = Tw_l1(i) + delTw1;
Tf_l1(i) = Tf_l1(i) + delTf1;
Tt_l1(i) = Tt_l1(i) + delTt1;
Tw1(j,i) = Tw_l1(i);
Tw_l2(i) = Tw_l2(i) + delTw2;
Tf_l2(i) = Tf_l2(i) + delTf2;
Tt_l2(i) = Tt_l2(i) + delTt2;
Tw2(j,i) = Tw_l2(i);

% Calculate martensite fraction profile
if j == 1
    Rm1(j,i) = 1;
    Rm2(j,i) = 1;
else

    % Determine curve from sign of temperature change
    % rate. See Thesis Eqn 2.21
    hf1 = .5*(1+erf((Tw1(j,i)-Abar)/(sa*sqrt(2)))); % Fwd
    hr1 = .5*(1+erf((Tw1(j,i)-Mbar)/(sm*sqrt(2)))); % Rev
    hf2 = .5*(1+erf((Tw2(j,i)-Abar)/(sa*sqrt(2)))); % Fwd
    hr2 = .5*(1+erf((Tw2(j,i)-Mbar)/(sm*sqrt(2)))); % Rev

    % Calculate Rm
    if delTw1 == 0
        Rm1(j,i) = Rm1(j-1,i);
    elseif delTw1 > 0
        g = exp(-(Tw1(j,i)-Abar)^2/(2*sa^2))/sa/sqrt(2*pi);
        Rm1(j,i) = Rm1(j-1,i)+(hr1+Rm1(j-1,i)-1)/(hf1-...
          hr1)*g*delTw1;
    elseif delTw1 < 0
        g = exp(-(Tw1(j,i)-Mbar)^2/(2*sm^2))/sm/sqrt(2*pi);
        Rm1(j,i) = Rm1(j-1,i)+(hf1+Rm1(j-1,i)-1)/(hr1-...
          hf1)*g*delTw1;
    end

    if delTw2 == 0
        Rm2(j,i) = Rm2(j-1,i);
    elseif delTw2 > 0
        g = exp(-(Tw2(j,i)-Abar)^2/(2*sa^2))/sa/sqrt(2*pi);
        Rm2(j,i) = Rm2(j-1,i)+(hr2+Rm2(j-1,i)-1)/(hf2-...
          hr2)*g*delTw2;
    elseif delTw2 < 0
        g = exp(-(Tw2(j,i)-Mbar)^2/(2*sm^2))/sm/sqrt(2*pi);
        Rm2(j,i) = Rm2(j-1,i)*(1+(hf2+Rm2(j-1,i)-1)/(hr2-...
          hf2)*g*delTw2);
    end

    if isnan(Rm1(j,i)) || abs(Rm1(j,i)) == Inf
        Rm1(j,i) = Rm1(j-1,i);
    elseif Rm1(j,i) < 0
        Rm1(j,i) = 0;
    elseif Rm1(j,i) > 1
        Rm1(j,i) = 1;
    end

    if isnan(Rm2(j,i)) || abs(Rm2(j,i)) == Inf
        Rm2(j,i) = Rm2(j-1,i);
    elseif Rm2(j,i) < 0
        Rm2(j,i) = 0;
```

```
            elseif Rm2(j,i) > 1
                Rm2(j,i) = 1;
            end

        end

    end

    % Fluid inlet temperature
    r = .8163;
    tau1 = .11;
    tau2 = .35;

    if ~count2
        Tfe1 = (Tfh-Tfc)*(r*(1-exp(-1/tau1*(t(j)-ts*count)))+(1-r)*...
            (1-exp(-1/tau2*(t(j)-ts*count))))+Tfc;
        Tfe2 = (Tfc-Tfh)*(r*(1-exp(-1/tau1*(t(j)-ts*count)))+(1-r)*...
            (1-exp(-1/tau2*(t(j)-ts*count))))+Tfh;
    else
        Tfe1 = (Tfc-Tfh)*(r*(1-exp(-1/tau1*(t(j)-ts*count)))+(1-r)*...
            (1-exp(-1/tau2*(t(j)-ts*count))))+Tfh;
        Tfe2 = (Tfh-Tfc)*(r*(1-exp(-1/tau1*(t(j)-ts*count)))+(1-r)*...
            (1-exp(-1/tau2*(t(j)-ts*count))))+Tfc;
    end

    if t(j) < 1
        Tfe2 = Ta;
    end

    % Advance Fluid for t_on seconds
    if cyc <= t_on
        Tf_l1 = [Tfe1 Tf_l1(1:n-1)];
        Tf_l2 = [Tfe2 Tf_l2(1:n-1)];
    end

end

for i = 1:n
    Rm1dot(:,i) = deriv(Rm1(:,i),t,1);
    Rm2dot(:,i) = deriv(Rm2(:,i),t,1);
end
```

B.4 Code for “pumpsys.m”

```
% This function returns the states of the SMA actuators and the pumping
% chambers.

function ydot = pumpsys(time,y)

global Rm1 Rm1dot Rm2 Rm2dot t n Ac Dw dx Sp C Rv R Ea M Ma
global eps1 eps2 epsdot1 epsdot2 sig1 sig2 sigdot1 sigdot2

% Interpolate martensite fraction
Rm1i = interp1(t,Rm1,time,'linear');
Rm1doti = interp1(t,Rm1dot,time,'linear');
Rm2i = interp1(t,Rm2,time,'linear');
Rm2doti = interp1(t,Rm2dot,time,'linear');

% Separate state variables
F1 = y(1:n);
F2 = y(n+1:2*n);
```

```
Pa = y(2*n+1);
Pb = y(2*n+2);
Vm = y(2*n+3);
Xm = y(2*n+4);

for i = 1:n

    % Calculate strains of each wire segment
    eps1(i) = dmartfracavg(Rm1i(i),F1(i));
    eps2(i) = dmartfracavg(Rm2i(i),F2(i));

    % Calculate strain rates of each wire segment
    if i == 1
        epsdot1(i) = 1/n*(Vm/dx + 1/R*(sum(F1(2:n)) - (n-1)*F1(1)));
        epsdot2(i) = 1/n*(-Vm/dx + 1/R*(sum(F2(2:n)) - (n-1)*F2(1)));
    else
        epsdot1(i) = 1/R*(1/n*(sum(F1) + R/dx*Vm) - F1(i));
        epsdot2(i) = 1/R*(1/n*(sum(F2) - R/dx*Vm) - F2(i));
    end

    % Calculate martensite phase stress
    sig1(i) = sigma(eps1(i));
    sig2(i) = sigma(eps2(i));

    % Calculate rate of change of martensite phase stress
    sigdot1(i) = sigmadot(eps1(i),epsdot1(i));
    sigdot2(i) = sigmadot(eps2(i),epsdot2(i));

    % Calculate force time derivatives
    Fdot1(i) = pi/4*Dw^2*Ea*((1-Rm1i(i))*epsdot1(i) -...
      Rm1doti(i)*eps1(i)) + pi/4*Dw^2*(Rm1i(i)*sigdot1(i) +...
      Rm1doti(i)*sig1(i));
    Fdot2(i) = pi/4*Dw^2*Ea*((1-Rm2i(i))*epsdot2(i) -...
      Rm2doti(i)*eps2(i)) + pi/4*Dw^2*(Rm2i(i)*sigdot2(i) +...
      Rm2doti(i)*sig2(i));

end

% Check valves
if Pa > Sp
    R1out = Rv;
else
    R1out = inf;
end

if Pa < 0
    R1in = Rv;
else
    R1in = inf;
end

if Pb > Sp
    R2out = Rv;
else
    R2out = inf;
end

if Pb < 0
    R2in = Rv;
else
    R2in = inf;
end

% Calculate forces at lever
```

```
Fa = Ac*Pa/Ma;  % Chamber 1 Pressure Force
Fb = Ac*Pb/Ma;  % Chamber 2 Pressure Force
Fc = 1/n*(sum(F1) + R/dx*Vm);   % Actuator 1 Force
Fd = 1/n*(sum(F2) - R/dx*Vm);   % Actuator 2 Force

% Calculate pressure rates of change
Padot = 1/C*(-1/R1out*(Pa-Sp) - 1/R1in*Pa + Ac*Vm/Ma);
Pbdot = 1/C*(-1/R2out*(Pb-Sp) - 1/R2in*Pb - Ac*Vm/Ma);

% Calculate velocity and position derivatives
Vmdot = 1/M*(Fb - Fa + Fd - Fc);
Xmdot = Vm;

% Calculate volume input and output
Vdot1 = 1/R1out*(Pa-Sp);
Vdot2 = 1/R2out*(Pb-Sp);
Vdot1in = -1/R1in*(Pa);
Vdot2in = -1/R2in*(Pb);

ydot = [Fdot1'; Fdot2'; Padot; Pbdot; Vmdot; Xmdot; Vdot1; Vdot2;
Vdot1in; Vdot2in];
```

B.5 Code for “sigma.m”

```
% This function returns the stress of the SMA actuator given the strain
% and is called by "pumpsys.m".

function y = sigma(eps)

global Em Et Ed eym edm

% See Eqn 2.25
if (eps < eym)
    y = Em*eps;
elseif (eps >= eym) & (eps < edm)
    y = Et*(eps-eym) + Em*eym;
elseif (eps >= edm)
    y = Ed*(eps-eym) + Et*(edm-eym) + Em*eym;
end
```

B.6 Code for “sigmadot.m”

```
% This function returns the strain rate given strain and strain rate
% and is called by "pumpsys.m".

function y = sigmadot(eps,epsdot)

global Em Et Ed eym edm

% See Eqn 2.28
if (eps < eym)
    y = Em*epsdot;
elseif (eps >= eym) & (eps < edm)
    y = Et*epsdot;
elseif (eps >= edm)
    y = Ed*epsdot;
end
```

APPENDIX C

LABVIEW INTERFACE USED FOR TESTING

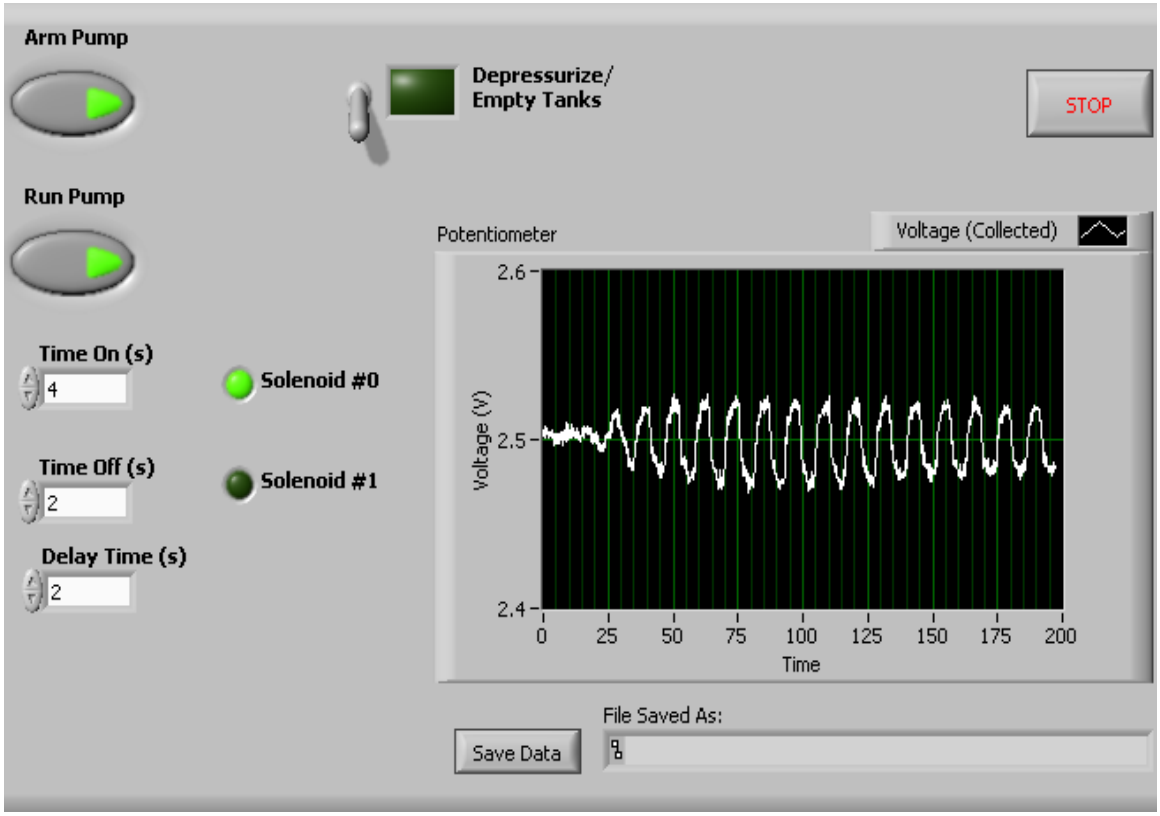

Figure C.1 LabVIEW front panel interface used for testing of the SMA pump.

REFERENCES

[1] I. W. Hunter and S. Lafontaine, "Comparison of muscle with artificial actuators," in *Proceedings - IEEE Solid-State Sensor and Actuator Workshop*, Hilton Head Island, SC, 1992, pp. 178-185.

[2] W. Haider, N. Munroe, C. Pulletikurthi, P. Gill, and S. Amruthaluri, "A Comparative Biocompatibility Analysis of Ternary Nitinol Alloys," *Journal of Materials Engineering and Performance*, vol. 18, pp. 760-764, 2009.

[3] K. T. O'Toole, M. M. McGrath, and E. Coyle, "Analysis and evaluation of the dynamic performance of SMA actuators for prosthetic hand design," in *Journal of Materials Engineering and Performance*, New York, NY, 2009, pp. 781-786.

[4] Y. Yam, K.-F. Lei, and P. Baranyi, "Control of a SMA actuated artificial face via neuro-fuzzy techniques," in *Proceedings - IEEE International Conference on Fuzzy Systems*, Melbourne, Australia, 2001, pp. 1315-1318.

[5] B. J. Huang, J. H. Wang, J. H. Wu, and P. E. Yang, "A fast response heat pump water heater using thermostat made from shape memory alloy," *Applied Thermal Engineering*, vol. 29, pp. 56-63, 2009.

[6] U. Icardi and L. Ferrero, "SMA actuated mechanism for an adaptive wing," *Journal of Aerospace Engineering*, vol. 24, pp. 140-143, 2011.

[7] Y. Tadesse, D. Hong, and S. Priya, "Twelve degree of freedom baby humanoid head using shape memory alloy actuators," *Journal of Mechanisms and Robotics*, vol. 3, 2011.

[8] R. Kratz, S. Klug, M. Stelzer, and O. Von Stryk, "Biologically inspired reflex based stabilization control of a humanoid robot with artificial SMA muscles," in *Proceedings - IEEE International Conference on Robotics and Biomimetics, ROBIO 2006*, Kunming, China, 2006, pp. 1089-1094.

[9] S. A. Mascaro and H. H. Asada, "Wet shape memory alloy actuators for active vasculated robotic flesh," in *Proceedings - IEEE International Conference on Robotics and Automation*, Taipei, Taiwan, 2003, pp. 282-287.

[10] O. K. Rediniotis, D. C. Lagoudas, H. Y. Jun, and R. D. Allen, "Fuel-powered

compact SMA actuator," in *Proceedings - 2002 SPIE Conference on Smart Structures and Materials*, San Diego, CA, United states, 2002, pp. 441-453.

[11] L. Flemming and S. Mascaro, "Analysis of hybrid electric/thermofluidic control for wet shape memory alloy actuators," in *Proceedings - ASME Dynamic Systems and Control Conference 2009, DSCC2009*, Hollywood, CA, United states, 2009, pp. 1041-1047.

[12] L. Flemming and S. Mascaro, "Wet SMA actuator array with matrix vasoconstriction device," in *Proceedings - ASME Dynamic Systems and Control Division*, Orlando, FL, United states, 2005, pp. 1751-1758.

[13] J. D. Ertel, "Design and modeling of a shape memory alloy actuated robotic heart," Salt Lake City, UT: University of Utah, 2007.

[14] J. D. Ertel and S. A. Mascaro, "Dynamic thermomechanical modeling of a wet shape memory alloy actuator," *Journal of Dynamic Systems, Measurement and Control, Transactions of the ASME*, vol. 132, pp. 1-9.

[15] N. P. Cheremisnoff and P. N. Cheremisnoff, *Pumps and Pumping Operations*. Englewood Cliffs, NJ: Prentice-Hall, Inc., 1992.

[16] P. Fraenkel, *Water Pumping Devices: A Handbook for Users and Choosers*, 2nd ed. Southampton, London, UK: Intermediate Technology Publications, 1997.

[17] J. Dong, W. Zheng, Z. Yang, B. Wu, B. Jiang, and X. Yao, "Research on push type piezoelectric insulin pump," in *Proceedings - IEEE International Conference on Mechatronics and Automation, ICMA 2009*, Changchun, China, 2009, pp. 186-191.

[18] B. Phibbs, *The Human Heart: A Basic Guide to Heart Disease*, 2nd ed. Philadelphia, PA: Lippincott, Williams & Wilkins, 2007.

[19] D. D. Shin, K. P. Mohanchandra, and G. P. Carman, "Development of hydraulic linear actuator using thin film SMA," *Sensors and Actuators, A: Physical*, vol. 119, pp. 151-156, 2005.

[20] E. Makino, T. Mitsuya, and T. Shibata, "Micromachining of TiNi shape memory thin film for fabrication of micropump," *Sensors and Actuators, A: Physical*, vol. 79, pp. 251-259, 2000.

[21] W. L. Benard, H. Kahn, A. H. Heuer, and M. A. Huff, "Titanium-nickel shape-memory alloy actuated micropump," in *Proceedings - International Conference on Solid-State Sensors and Actuators*, Chicago, IL, 1997, pp. 361-364.

[22] W. L. Benard, H. Kahn, A. H. Heuer, and M. A. Huff, "Thin-film shape-memory

alloy actuated micropumps," *Journal of Microelectromechanical Systems*, vol. 7, pp. 245-251, 1998.

[23] S. Guo, X. Sun, K. Ishii, and J. Guo, "SMA actuator-based novel type of peristaltic micropump," in *Proceedings - IEEE International Conference on Information and Automation, ICIA 2008*, Zhangjiajie, Hunan, China, 2008, pp. 1620-1625.

[24] X. Sun, S. Guo, and Y. Xiaonan, "A Novel type of peristaltic micropump for biomedical applications," Takamatsu, Japan, 2008, pp. 696-701.

[25] X. Sun, S. Guo, X. Ye, and Y. Hao, "A new type of compound peristaltic micropump," Harbin, China, 2008, pp. 51-54.

[26] K. Ikuta, A. Takahashi, K. Ikeda, and S. Maruo, "Fully integrated micro biochemical laboratory using biochemical IC chips - Cell-free protein synthesis by using a built-in micropump chip," in *Proceedings - IEEE Micro Electro Mechanical Systems (MEMS)*, Kyoto, Japan, 2003, pp. 451-454.

[27] K. Ikuta, T. Hasegawa, and T. Adachi, "SMA micro pump chip to flow liquids and gases," Tsukuba, Japan, 2008, pp. 343-350.

[28] MetalBellows.com. (2011, Mar 9) *OTS Bellows: Off-The-Shelf Welded Diaphragm Metal Bellows* [Online] Available: http://www.metalbellows.com/documents/OTS_Bellows.pdf

[29] EngineeringToolbox.com. (2011, Feb 10) *Boiling Point of Water at Various Elevations* [Online] Available: http://www.engineeringtoolbox.com/boiling-points-water-altitude-d_1344.html

[30] Dow.com. (2011, Feb 10) *Vapor Pressure and Boiling Point* [Online] Available: http://www.dow.com/glycerine/resources/vappress.htm

[31] F. P. Incropera, D. P. DeWitt, T. L. Bergman, and A. S. Lavine, *Fundamentals of Heat and Mass Transfer*, 6th ed. Hoboken, NJ: John Wiley & Sons, Inc., 2007.

[32] Y. A. Çengal and M. A. Boles, *Thermodynamics, An Engineering Approach*, 5th ed. New York, NY: McGraw-Hill, 2006.

[33] S. M. Dutta and F. H. Ghorbel, "Differential Hysteresis Modeling of a Shape Memory Alloy Wire Actuator," *IEEE/ASME Transactions on Mechatronics*, vol. 10, no. 2, pp. 189-197, 2005.

[34] M. Kadkhodaei, R. K. N. D. Rajapakse, M. Mahzoon, and M. Salimi, "Modeling of the cyclic thermomechanical response of SMA wires at different strain rates," *Smart Materials and Structures*, vol. 16, pp. 2091-2101, 2007.

[35] J. Abadie, N. Chaillet, and C. Lexcellent, "Modeling of a new SMA micro-actuator for active endoscopy applications," *Mechatronics,* vol. 19, pp. 437-442, 2009.

[36] CatPumps.com. (2011, Feb 18) *3 Frame Piston Pump Brass Models* [Online] Available: http://www.catpumps.com/select/pdfs/280.pdf

[37] BoschRexroth.com. (2011, Feb 18) *Bosch Rexroth Mobile Hydraulics* [Online] Available: http://www.boschrexroth.com/mobile-hydraulics-catalog/Vornavigation/VorNavi.cfm?Language=EN&PageID=m3439

[38] ColeParmer.com. (2011, Feb 18) *Cole-Parmer Virtual Catalog* [Online] Available: http://www.coleparmer.com/catalog/vcatalog_page.asp?p=01643

[39] Annovi-Reverberi.com. (2011, Feb 18) *AR North America - RMV2.5G20D - 3400 rpm* [Online] Available: http://www.annovi-reverberi.com/rmpumps/rmv25g20dpg1.html

[40] Annovi-Reverberi.com. (2011, Feb 18) *AR North America - SJV 3400 rpm Breakdown* [Online] Available: http://www.annovi-reverberi.com/xjsjpumps/sjv3400bd.html

[41] Sauer-Danfoss.com. (2011, Feb 18) *Series 45 Axial Piston Open Circuit Pumps* [Online] Available: http://www.sauer-danfoss.com/stellent/groups/publications/documents/product_literature/520l0519.pdf

[42] IRTechPubs.com. (2011, Feb 18) *Sales & Engineering Data - 650939-X4D-B Two Ball Pump* [Online] Available: http://www.irtechpubs.com/ir_pdfs/Fluid%20Technologies/ARO%20Fluid%20Products/Piston%20Pumps%20Sales%20%26%20Engineering%20Data/650939-XXX-B-SE.pdf

[43] IMO-Pump.com. (2011, Feb 18) *IMO Pump - Model 3E* [Online] Available: http://www.imo-pump.com/Brochures/BR00003E.PDF

[44] IMO-Pump.com. (2011, Feb 18) *IMO Pump - Model 6T/6U* [Online] Available: http://www.imo-pump.com/brochures/BR006T6U.PDF

[45] LeistritzCorp.com. (2011, Feb 18) *L3 Standard Lube Oil Pump* [Online] Available: http://www.leistritzcorp.com/pdf/lubeoilpump.pdf

[46] WarrenPumps.com. (2011, Feb 18) *Warren Pumps - Medium Pressure* [Online] Available: http://www.warrenpumps.com/industrial/mediumpressure.htm

[47] Graco.com. (2011, Feb 18) *Process Equipment Catalog - Solutions for Industrial Applications* [Online] Available: http://wwwd.graco.com/Distributors/

DLibrary.nsf/Files/300435/$file/300435J.pdf

[48] WildenPump.com. (2011, Feb 18) *P100 - Engineering Operation & Maintenance* [Online] Available: http://www.wildenpump.com/files/products/P100-ADV-PLS-EOM-02.pdf

[49] Drillspot.com. (2011, Feb 18) *Flojet 01200-12C* [Online] Available: http://www.drillspot.com/products/77404/Flojet_02100-12C_Automatic_Marine_RV_Pump

[50] GrundfosAlldos.com. (2011, Feb 18) *Grundfos Alldos Data Booklet - DME and DMS* [Online] Available: http://www.grundfosalldos.com/e/html/02_produkte/1103_dme_2_380.php

[51] Hydra-Cell.com. (2011, Feb 18) *Hydra-Cell Products F/G-20* [Online] Available: http://www.hydra-cell.com/product/F20-hydracell-pump.html

[52] PlumberSurplus.com. (2011, Feb 18) *Little Giant 1-A 170 GPH Small Submersible* [Online] Available: http://www.plumbersurplus.com/Prod/Little-Giant-1-A-170-GPH-Small-Submersible-6-Cord-%28500203%29/56728/Cat/773?gclid=CLz7lr7lsqcCFRFOgwodThAPBw

[53] Drillspot.com. (2011, Feb 18) *Dayton 4HFA7 Booster Pump* [Online] Available: http://www.drillspot.com/products/1320047/Booster_Pump_4HFA7_Booster_Pump

[54] Drillspot.com. (2011, Feb 18) *Dayton 2YEV3 Chemical-Resistant Pedestal Pump* [Online] Available: http://www.drillspot.com/products/552075/dayton_2yev3_chemical-resistant_pedestal_pump

[55] Drillspot.com. (2011, Feb 18) *Dayton 2ZWZ1 Centrifugal Pedestal Pump* [Online] Available: http://www.drillspot.com/products/489560/dayton_2zwz1_centrifugal_pedestal_pump

[56] NorthernTool.com. (2011, Feb 18) *IPT Two-Stage Sprinkler Booster Pump* [Online] Available: http://www.northerntool.com/shop/tools/product_200390330_200390330